Linked-Pair Expansions in Quantum Statistics*

FRANZ MOHLING†
Department of Physics, Columbia University, New York, New York
(Received July 21, 1960)

In the quantum statistical method of Lee and Yang, the cluster functions of quantum statistics are expressed in terms of the cluster functions of Boltzmann statistics, which in turn are computed in terms of certain two-body functions. In the present paper, following a detailed study of the Boltzmann cluster functions, it is shown that the symmetric representation can be used for the two-body functions and that large classes of diagrams can be summed. This leads to the introduction of linked-pair graphs to describe the functions of quantum statistics. The two-body functions are expressed in terms of two-body wave functions, and are therefore well-defined for hard-core repulsions. For weak potentials the method is shown to be equivalent to the theory of Bloch and DeDominicis.

INTRODUCTION

CONSIDERABLE attention has been devoted in recent years to the development of systematic methods for calculating the low-temperature properties of many-body systems. Generally speaking, there exist two approaches to such problems, namely generalized perturbation theoretic methods and the methods of quantum statistical mechanics. In this paper we discuss only the latter.

The central problem of quantum statistics is the determination of the logarithm of the grand partition function, i.e., the grand potential $f^{(s)}$, because with a knowledge of the grand potential one may calculate all quantities of physical interest in a large system of particles. A standard approach to the problem is to use the well-known method of Ursell to express the grand potential in terms of integrals over cluster functions.[1] An important development in this drection has recently been made by Lee and Yang,[2] who have shown that the cluster functions of quantum statistics, $U_N^{(s)}$, can be expressed in terms of the unsymmetrized cluster functions of Boltzmann statistics, U_N, which Lee and Yang have in turn reduced to a series of quadratures over two-body cluster functions. Subsequently, in a remarkable series of papers[3] these authors have applied their method to the calculation of the low-temperature properties of a Bose gas of hard spheres. They have also shown how to calculate the thermodynamics of a Fermi gas of hard spheres at low temperatures.

In an investigation of the higher order corrections to the thermodynamics of a Fermi gas, one finds that the method of Lee and Yang involves extremely tedious combinatorial problems. Lee and Yang have simplified this problem somewhat in their paper IV,[3] and we use their results as a starting point for this paper. It is shown that a systematic study of the unsymmetrized cluster functions leads to a linked-pair expansion of the grand potential in which the combinatorial problems of the Lee-Yang method are considerably simplified. More important, however, the linked-pair formulation is an essential step in the calculation of the momentum distribution of a Fermi gas, as we shall show in the following paper.

In Sec. I, the equations of quantum statistics are reviewed within the framework of the method of Lee and Yang. In particular, the basic equations which occur in the theory of the grand canonical ensemble are first presented and then the method of Ursell is briefly outlined. Section I concludes with Eqs. (21) and (22), which express the grand potential of quantum statistics in terms of contracted 0-graphs (LY IV).[3] In order to simplify subsequent analysis, all expressions are written in the interaction representation.

The detailed study of the Boltzmann cluster functions is initiated in Sec. II, following a method due to Jacobsohn.[4] In analogy with Lee and Yang,[2] X diagrams are introduced to represent the temperature integrals over products of two-particle cluster functions mentioned above. In the X diagram notation, symmetrized combinations of the two-particle functions do not explicitly appear. However, using the notation of dashed-line cluster graphs, which we introduce, it is possible to express a symmetric combination T_N of the Boltzmann cluster functions U_N in terms of integrals over products of *symmetrized matrix elements* of the two-particle cluster functions, which we call *pair functions*. The T_N, incidentally, are not equal to the cluster functions of quantum statistics, i.e., $T_N \neq U_N^{(s)}$, since they do not include the effect of wave function overlap due to thermal motion. The principle result of Sec. II is Eq. (47) for the T_N.

Section III is devoted to the rather complicated process of summing over the large class of dashed-line cluster graphs which consist of all ways of including "double bonds" in a given cluster graph. This is the

* Work supported in part by the U. S. Atomic Energy Commission.
† Now at Cornell University, Ithaca, New York.
[1] B. Kahn and G. E. Uhlenbeck, Physica **5**, 399 (1938). See also D. ter Haar, *Elements of Statistical Mechanics*, (Rinehart and Company, New York, 1954), Chaps. VII and VIII.
[2] T. D. Lee and C. N. Yang, Phys. Rev. **113**, 1165 (1959)-(LY I).
[3] T. D. Lee and C. N. Yang, Phys. Rev. **116**, 25 (1959)-(LY II); **117**, 12 (1960)-(LY III); **117**, 22 (1960)-(LY IV); **117**, 897 (1960)-(LY V).
[4] F. Mohling, thesis, University of Washington, 1958 (unpublished).

step which is essential to the investigations described in the following paper, and it leads to the introduction of wiggly-line cluster graphs. In the final relation of this section, Eq. (54), the T_N are expressed in terms of these wiggly-line cluster graphs, instead of the dashed-line cluster graphs.

The linked-pair expansion of the grand potential, Eq. (57), is derived in Sec. IV by substituting Eq. (54) for the T_N into Eq. (21) for $f^{(s)}$. The linked-pair formulation is therefore merely an extension of the contracted 0-graph formulation of Lee and Yang. It is also quite closely related to the method of Bloch and DeDominicis,[5] which is another of the methods of quantum statistics. The correspondence is established at the end of Sec. IV by expanding the pair function in terms of the two-body potential.

In the theory of Bloch and DeDominicis the grand potential is expressed in terms of the two-body potential. It is therefore only a useful theory when the two-body potential is truly weak. This is not the case, however, for any system in which a hard core repulsion is an important part of the two-body interaction. On the other hand, the pair functions of the present paper, and the corresponding two-body functions of Lee and Yang, are well-suited for dealing with strong, short-range interactions. Thus, in Sec. V it is shown that the pair-functions can be expressed entirely in terms of two-particle wave functions, which, of course, are finite and well-behaved for all interactions.

Because of the complexity of the derivations outlined in this paper, a large number of examples and figures have been included. Also, the momentum representation has been used almost exclusively, for reasons of clarity and simplicity.

I. A REVIEW OF THE EQUATIONS OF QUANTUM STATISTICS

The theory of the grand canonical ensemble becomes useful when one is interested in calculating not only the average energy of a system, but also the average density and its fluctuations. For a system in which the only conserved quantities are the energy E and the total number of particles N, the grand partition function is

$$e^{\Omega f}=\sum_{N=0}^{\infty} z^N \operatorname{Tr}_N[\exp(-\beta H^{(N)})], \tag{1}$$

where

$$\beta=1/kT, \tag{2}$$

and Ω is the volume of the system. The symbol Tr_N indicates that the trace of $\exp[-\beta H^{(N)}]$ is to be taken over a complete set of N-particle state vectors. Moreover, we shall assume that the N-particle Hamiltonian $H^{(N)}$ includes only two-particle interactions. The quantity f is called the grand potential and it is assumed to be an intensive quantity, i.e., we assume that $\lim f(z,\Omega,\beta)$ for $\Omega\to\infty$ exists. Finally, the fugacity z can be shown to be related to the thermodynamic (or Gibbs) potential per particle g by the equation

$$z=e^{\beta g}. \tag{3}$$

In terms of the independent variables β and g, the thermodynamic properties of a system of particles can be determined using the following equations:

Pressure,

$$\mathcal{P}=\beta^{-1}\frac{\partial}{\partial\Omega}(\Omega f). \tag{4}$$

Particle density,

$$\rho=\langle N\rangle/\Omega=\beta^{-1}\partial f/\partial g. \tag{5}$$

Energy per particle,

$$\langle E\rangle/\langle N\rangle=g-\rho^{-1}(\partial f/\partial\beta). \tag{6}$$

These equations relate the thermodynamic properties of a system to the grand potential, which with the aid of the well-known Ursell method[1] can be written directly in terms of certain cluster integrals $b_N{}^{(s)}(\Omega,\beta)$:

$$f^{(s)}(z,\Omega,\beta)=\sum_{N=1}^{\infty} z^N b_N{}^{(s)}(\Omega,\beta). \tag{7}$$

In Eq. (7) the superscript (s) indicates that for quantum statistics the complete set of state vectors to be used in Eq. (1) must be symmetrized or antisymmetrized.

Our first departure from the treatment of Lee and Yang is that we employ the interaction representation in obtaining expressions for the cluster integrals. Let us define an operator

$$W_N(\beta)\equiv\exp(\beta H_0{}^{(N)})\exp(-\beta H^{(N)}), \tag{8}$$

which is equivalent to unity for free particles.[6] If one writes the matrix elements of $W_N(\beta)$ as

$$W^{(s)}\begin{pmatrix}1\,2\cdots N\\ 1'2'\cdots N'\end{pmatrix}\equiv\langle 12\cdots N|\,W_N{}^{(s)}(\beta)\,|1'2'\cdots N'\rangle$$
$$=\sum_{P'}\epsilon^{P'}P'\langle 12\cdots N|\,W_N(\beta)\,|1'2'\cdots N'\rangle, \tag{9}$$

where $\epsilon=+1$ for Bose-Einstein statistics and $\epsilon=-1$ for Fermi-Dirac statistics, and $\sum_{P'}$ denotes the sum over all permutations of the primed indices, then the grand partition function is given in terms of the $W_N{}^{(s)}$ as follows:

$$\exp(\Omega f^{(s)})=\sum_{N=0}^{\infty}\frac{z^N}{N!}\sum_{\mathbf{k}_1\cdots\mathbf{k}_N}\exp(-\beta\sum_{i=1}^{N}\omega_i)$$
$$\times W^{(s)}\begin{pmatrix}\mathbf{k}_1\mathbf{k}_2\cdots\mathbf{k}_N\\ \mathbf{k}_1\mathbf{k}_2\cdots\mathbf{k}_N\end{pmatrix}, \tag{10}$$

where $\omega_i=\hbar^2k_i^2/2m$.[7] For convenience, in Eq. (10) we

[5] C. Bloch and C. DeDominicis, Nuclear Phys. **7**, 459 (1958).

[6] We assume in this development that there are no applied external fields.

[7] Strictly speaking, the right-hand side of Eq. (9) should include an additional factor $\Pi_{k=1}{}^{N}(N_k!)^{-1}$, where for a wave function which is a product of single particle functions the N_k are the numbers of particles in each of the different states, but this factor cancels out in the derivation of Eq. (10).

have chosen the momentum representation for the sum over states, since the free particle operator $\exp[-\beta H_0^{(N)}]$ is diagonal in this representation. Now, the Ursell method consists of defining "cluster functions" $U_N^{(s)}$ in terms of the $W_N^{(s)}$ by the following set of equations:

$$
\begin{aligned}
&W^{(s)}\binom{1}{1'}=U^{(s)}\binom{1}{1'},\\
&W^{(s)}\binom{1\,2}{1'2'}\equiv U^{(s)}\binom{1}{1'}U^{(s)}\binom{2}{2'}+U^{(s)}\binom{1\,2}{1'2'},\\
&W^{(s)}\binom{1\,2\,3}{1'2'3'}\equiv U^{(s)}\binom{1}{1'}U^{(s)}\binom{2}{2'}U^{(s)}\binom{3}{3'}+U^{(s)}\binom{1}{1'}U^{(s)}\binom{2\,3}{2'3'}\\
&\qquad\qquad +U^{(s)}\binom{2}{2'}U^{(s)}\binom{3\,1}{3'1'}+U^{(s)}\binom{3}{3'}U^{(s)}\binom{1\,2}{1'2'}+U^{(s)}\binom{1\,2\,3}{1'2'3'},\ \text{etc.}
\end{aligned}
\tag{11}
$$

These equations are such that the Nth equation connects $W_N^{(s)}$ with all of the $U_1^{(s)}, U_2^{(s)}, \cdots U_N^{(s)}$. Without modifications they are only useful for systems in which the particle interactions have a finite range, and in this case the equations have the significance that they represent all possible ways in which N particles can be grouped into clusters which are *both* noninteracting and have nonoverlapping wave functions. Thus the $U_N^{(s)}$ are indeed "physical cluster functions," and one can show that the cluster integrals $b_N^{(s)}(\Omega,\beta)$ are given by

$$
b_N^{(s)}(\Omega,\beta)=(\Omega N!)^{-1}\sum_{\mathbf{k}_1\cdots\mathbf{k}_N}\exp(-\beta\sum_{i=1}^{N}\omega_i)\times U^{(s)}\binom{\mathbf{k}_1\mathbf{k}_2\cdots\mathbf{k}_N}{\mathbf{k}_1\mathbf{k}_2\cdots\mathbf{k}_N}, \tag{12}
$$

in the momentum representation.

The quantity which is a measure of the spread of particle wave functions is the thermal wavelength,

$$
\lambda_T=(2\pi\hbar^2/mkT)^{\frac{1}{2}}=(2\pi\hbar^2\beta/m)^{\frac{1}{2}}. \tag{13}
$$

For example, one can show in the Heisenberg and position representation that the one-particle cluster function is given simply by the expression

$$
\langle\mathbf{r}|\exp(-\beta H_0)|\mathbf{r}'\rangle=\lambda_T^{-3}\exp[-\pi\lambda_T^{-2}(\mathbf{r}-\mathbf{r}')^2]\underset{\lambda_T\to 0}{\longrightarrow}\delta^{(3)}(\mathbf{r}-\mathbf{r}'). \tag{14}
$$

The expression (14) can be understood better when one separates the effect of particle interactions from that of overlapping wave functions, i.e., from statistics, in the $U_N^{(s)}$. For this purpose one defines with Eqs. (11) the corresponding set of "unsymmetrized cluster functions" U_N of Boltzmann statistics. Now, the U_N contain only the effect of particle interactions, since they are defined with unsymmetrized wave functions. Moreover, it is a straightforward matter to solve for the $U_N^{(s)}$ in terms of the U_N using Eqs. (9) and (11). Thus, for example, for the two-particle cluster function one readily obtains

$$
U^{(s)}\binom{1\,2}{1'2'}=T\binom{1\,2}{1'2'}+\epsilon U\binom{1}{2'}U\binom{2}{1'}, \tag{15}
$$

where $\langle 12|T_2|1'2'\rangle$ comprises a symmetrized or antisymmetrized combination of $\langle 12|U_2|1'2'\rangle$ and $\langle 12|U_2|2'1'\rangle$, namely:

$$
T\binom{1\,2}{1'2'}\equiv U\binom{1\,2}{1'2'}+\epsilon U\binom{1\,2}{2'1'}. \tag{16}
$$

One sees then that the effect of overlapping wave functions is that $U_2^{(s)}$ contains not only $T(12;1'2')$, but also "coupled" one-particle cluster functions. According to Eq. (14), a measure of the importance of the term $\epsilon U(1;2')U(2;1')$ is the thermal wavelength λ_T.

It is clear from the structure of Eqs. (9) and (11) that in general $U_N^{(s)}$ may be expressed in terms of sums over "connected products" of symmetric or antisymmetric T functions, where

$$
T\binom{1\,2\cdots N}{1'2'\cdots N'}\equiv\epsilon^N\sum_{P'}\epsilon^{P'}P'U\binom{1\,2\cdots N}{1'2'\cdots N'}. \tag{17}
$$

The factor ϵ^N has been introduced for convenience in later manipulations. Thus, using Eqs. (7) and (12), the grand potential $f^{(s)}$ may be expressed in terms of a sum over *all* connected products of T functions. The exact character of this sum is most simply described in terms of primary 0-graphs, as introduced by Lee and Yang (LY IV).[3] These graphs, as well as the corresponding ζ graphs for $\zeta>0$, which are needed in the calculation of distribution functions, are defined in the following two paragraphs.

A *primary ζ graph* ($\zeta=0, 1, 2\cdots$) consists of a collection of vertices connected by directed lines, with ζ external incoming lines and ζ external outgoing lines. Each vertex is characterized by a number α ($\alpha=1, 2, \cdots$) which gives the number of incoming and the number of

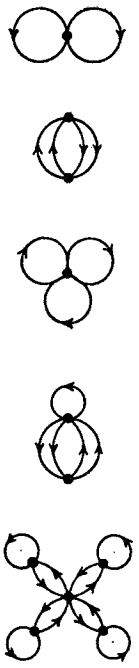

FIG. 1. Some examples of contracted 0-graphs. With each graph has been included its inverse symmetry number S^{-1}. [In (LY IV), dashed lines are used for these graphs].

outgoing lines at that vertex. Two primary graphs are different if their topological structures are different.

To each primary ζ graph we assign a term which is determined by the following procedures:

(i) Associate with each internal line a different integer i ($i=1, 2, \cdots m$) and a corresponding momentum $\mathbf{k}_i$.

(ii) If $\zeta \neq 0$ then associate the external lines with certain pre-given momenta.

(iii) To each α vertex, assign a factor

$$T\begin{pmatrix}\mathbf{k}_{A1}\cdots\mathbf{k}_{A\alpha}\\ \mathbf{k}_{B1}\cdots\mathbf{k}_{B\alpha}\end{pmatrix},$$

where $\mathbf{k}_{B1}\cdots\mathbf{k}_{B\alpha}$ are the momenta associated with its incoming lines and $\mathbf{k}_{A1}\cdots\mathbf{k}_{A\alpha}$ are the momenta associated with its outgoing lines.

(iv) Assign a factor $\epsilon e^{\beta(g-w_k)}$ to each *internal* line, where $w_k=\hbar^2k^2/2M$ is the energy variable for that line.[8]

(v) Assign a factor S^{-1} to the entire graph, where

$$S=\text{symmetry number}. \tag{18}$$

The symmetry number is defined to be the total number of permutations of the m integers associated with the internal lines that leave the graph topologically (including the positions of these numbers relative to the lines) unchanged.

(vi) Assign an over-all sign ϵ^{P_B} to the entire graph, where P_B is the permutation of the $(m+\zeta)$ bottom row coordinates (in the T product) with respect to the $(m+\zeta)$ top row coordinates.

(vii) Finally, sum over all the internal momenta $\mathbf{k}_1, \mathbf{k}_2, \cdots \mathbf{k}_m$.

With these definitions the grand potential $f^{(s)}$ is given in the momentum representation by:

$$\Omega f^{(s)}(g,\Omega,\beta)=\sum \text{(all different primary 0-graphs)}. \tag{19}$$

For further discussion and examples the reader is referred to Sec. 3 of (LY IV).[3]

Now, each 1-vertex corresponds to a factor $U_1=1$. It is therefore a simple matter to sum over all ways of including 1-vertices along the internal lines of any primary ζ graph which originally has no 1-vertices. The result of such a sum has been defined by Lee and Yang to be a contracted ζ graph. More precisely, *contracted ζ graphs* are calculated in the same manner as primary ζ graphs except that

(1) there are no 1-vertices in contracted ζ graphs.
(2) rule (iv) is replaced by
(iv)′ Assign a factor $\epsilon\nu_k$ to each internal line, where

$$\nu_k\equiv\frac{e^{\beta(g-w_k)}}{1-\epsilon e^{\beta(g-w_k)}}. \tag{20}$$

In terms of contracted 0-graphs, the grand potential is given by

$$\Omega f^{(s)}(g,\Omega,\beta)\equiv\Omega f_0{}^{(s)}(g,\Omega,\beta) + \sum \text{(all different contracted 0-graphs)}, \tag{21}$$

where

$$f_0{}^{(s)}(g,\Omega,\beta)\equiv -\epsilon\Omega^{-1}\sum_k \ln[1-\epsilon e^{\beta(g-w_k)}]. \tag{22}$$

Some examples of contracted 0-graphs are shown in Fig. 1 together with their inverse symmetry numbers S^{-1}. In this paper, we will not be concerned with ζ graphs for $\zeta>0$.

II. THE T_N IN TERMS OF TWO-BODY FUNCTIONS

Equation (21) is useful if one can calculate the unsymmetrized cluster functions $\langle 12\cdots N|U_N|1'2'\cdots N'\rangle$ or at least the $\langle 12\cdots N|T_N|1'2'\cdots N'\rangle$, in an explicit manner. This is indeed the case, for Lee and Yang[2] have shown that the $U_N(\beta)$ can be written entirely in terms of two-body wave functions, a result which they have applied in their studies of a gas of hard spheres. We shall now outline a new derivation of their results, due in part to Jacobsohn,[4] which we shall then extend to arrive at the "linked-pair expansion" of $f^{(s)}$. The reader should recall throughout that we are using the interaction representation.

We begin by defining an operator

$$W_N(\beta,\beta')\equiv\exp(\beta H_0{}^{(N)})\exp(-\beta H^{(N)}) \times\exp(\beta' H^{(N)})\exp(-\beta' H_0{}^{(N)}), \tag{23}$$
$$W_N(\beta,\beta)=1,$$

[8] The apparent difference between our rule (iv) and the corresponding rule (iv) of Lee and Yang is due to our use of the interaction representation.

which reduces to $W_N(\beta)$ for $\beta'=0$. In the development below we shall first show how $W_N(\beta,\beta')$ can be expanded into an infinite series of two-body operators. When this series is appropriately grouped, it becomes clear that the various groups are in one-to-one correspondence with the terms of the Nth Ursell equation (11) (as written for Boltzmann statistics). It is then easy to identify an operator $U_N(\beta,\beta')$ whose matrix elements (for $\beta'=0$) are exactly the unsymmetrized cluster functions.

The operator $W_N(\beta,\beta')$ has a simple transitive property:

$$W_N(\beta_1,\beta_2)W_N(\beta_2,\beta_3)=W_N(\beta_1,\beta_3). \tag{24}$$

Moreover, it satisfies the differential equations,

$$\begin{aligned}\frac{\partial}{\partial\beta}W_N(\beta,\beta')&=-\mathbf{V}_N(\beta)W_N(\beta,\beta'),\\ \frac{\partial}{\partial\beta'}W_N(\beta,\beta')&=W_N(\beta,\beta')\mathbf{V}_N(\beta'),\end{aligned} \tag{25}$$

where

$$\begin{aligned}\mathbf{V}_N(\beta)&\equiv\exp(\beta H_0^{(N)})\mathbf{V}_N\exp(-\beta H_0^{(N)}),\\ \mathbf{V}_N&=\textstyle\sum_\mu V_\mu.\end{aligned} \tag{26}$$

The subscript μ refers to a coordinate-pair chosen from the N coordinates. The summation over μ indicates the summation over all $\frac{1}{2}N(N-1)$ pairs.

Watson and Riesenfeld[9] have shown that differential equations such as (25), in which the $\mathbf{V}_N$ are given by Eqs. (26), are equivalent to the following set of integral equations:

$$\begin{aligned}W_N(\beta,\beta')&=1-\sum_\mu\int_{\beta'}^{\beta}dt\,W_2{}^\mu(\beta,t)\mathbf{V}_\mu(t)M_\mu{}^{(N)}(t,\beta'),\\ M_\mu{}^{(N)}(\beta,\beta')&=1-\sum_{\nu\neq\mu}\int_{\beta'}^{\beta}dt\,W_2{}^\nu(\beta,t)\mathbf{V}_\nu(t)M_\nu{}^{(N)}(t,\beta').\end{aligned} \tag{27}$$

It is readily verified that the $W_N(\beta,\beta')$ of Eq. (27) satisfies the differential equations (25) together with the initial condition $W_N(\beta,\beta)=1$.

It is an important feature of the Lee-Yang method of quantum statistics that it expresses the unsymmetrized cluster functions in terms of two-particle wave functions and not in terms of potentials, since the latter may be highly singular (as for hard-core repulsions) whereas the former are always well-behaved. In the present treatment we must also remove the explicit appearance of the operator $\mathbf{V}(t)$ in Eqs. (27). We therefore introduce an operator

$$R(\beta,\beta')\equiv-\frac{\partial}{\partial\beta'}W_2(\beta,\beta')=-W_2(\beta,\beta')\mathbf{V}(\beta'), \tag{28}$$

[9] W. B. Riesenfeld and K. M. Watson, Phys. Rev. **104**, 492 (1956).

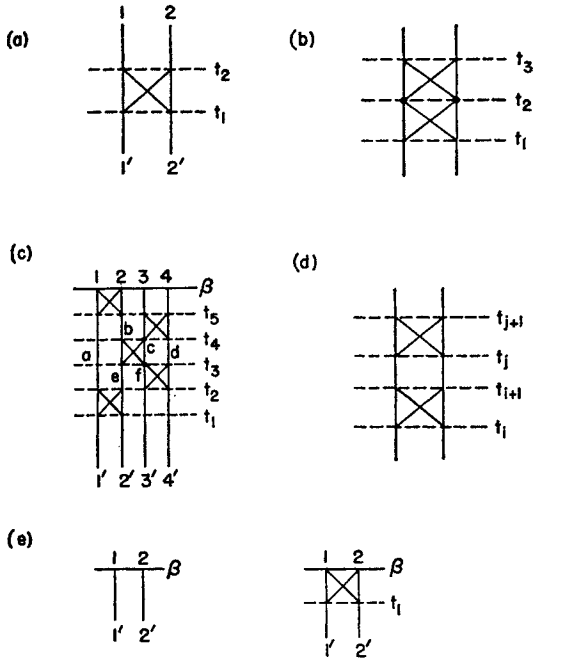

FIG. 2. (a) The symbol for the matrix elements of $R(t_2,t_1)$, see Eq. (30); (b) a forbidden structure in X diagrams; (c) a typical fifth order X diagram for four particles, see Eq. (31); (d) a double bond in X diagrams; (e) the two X diagrams in $\langle 12|W_2(\beta)|1'2'\rangle$.

and in Sec. V we shall show that the matrix elements of $R(\beta,\beta')$ can be expressed entirely in terms of two-body wave functions. Thus, we replace Eqs. (27) by

$$\begin{aligned}W_N(\beta)&=1+\sum_\mu\int_0^\beta dt\,R_\mu(\beta,t)M_\mu{}^{(N)}(t),\\ M_\mu{}^{(N)}(\beta)&=1+\sum_{\nu\neq\mu}\int_0^\beta dt\,R_\nu(\beta,t)M_\nu{}^{(N)}(t).\end{aligned} \tag{29}$$

In Eqs. (29) we have set $\beta'=0$, since it is no longer necessary to carry along the extra variable β'.

X-Diagrams

Equations (29) may be solved by iteration, and in any particular representation the result may be easily described in terms of X *diagrams*. The basic unit of an X diagrams is the symbol of Fig. 2(a) for the matrix elements of $R(t_2,t_1)$.

$$[\text{symbol of Fig. 2(a)}]=\langle 12|R(t_2,t_1)|1'2'\rangle = {}^{t_2}\binom{1\,2}{1'2'}_{t_1}={}^{t_2}\binom{2\,1}{2'1'}_{t_1}. \tag{30}$$

The X diagrams associated with the N-particle matrix elements of $W_N(\beta)$ for $N\geq 2$ are formed by first drawing N vertical lines and labeling them from left to right at the top from 1 to N and at the bottom from 1′ to

N'. One horizontal line labeled β is then drawn at the top of the diagram, and $Q \geq 0$ horizontal lines, labeled $(t_1, t_2, \cdots t_Q)$ from bottom to top, are drawn below this line. An X diagram is completed by inserting the crosses of Fig. 2(a) in the boxes formed, according to the following two rules.

(1) One and only one cross can occur between any two horizontal lines.

(2) Two crosses can never have two points in common, i.e., the structure of Fig. 2(b) is forbidden.

The number Q is defined to be the *order* of the X diagram, and it is equal to the number of crosses which the diagram contains.

A typical fifth-order X diagram for four particles is shown in Fig. 2(c), and its explicit expression is as follows:

$$[X \text{ diagram of Fig. 2(c)}] = (+1) \sum_{abcdef} \int_0^\beta dt_5 \int_0^{t_5} dt_4 \int_0^{t_4} dt_3 \int_0^{t_3} dt_2 \int_0^{t_2} dt_1 \times {}^{\beta}\binom{12}{ab}_{t_5}{}^{t_5}\binom{34}{cd}_{t_4}{}^{t_4}\binom{bc}{ef}_{t_3}{}^{t_3}\binom{f\,d}{3'4'}_{t_2}{}^{t_2}\binom{a\,e}{1'2'}_{t_1}. \quad (31)$$

In this expression, the "internal" coordinates, which arise from the sums over intermediate states in any particular representation, are labelled with lower case letters. The Q temperature integrations are over the interval from 0 to β such that $0 < t_1 < t_2 < t_3 \cdots < t_Q < \beta$. It follows from the above definition of an X diagram that the matrix elements of Eqs. (29) can be written as follows:

$$\langle 12\cdots N | W_N(\beta) | 1'2'\cdots N' \rangle = \sum_{Q=0}^{\infty} [\text{all different } Q\text{th-order } X \text{ diagrams for } N \text{ particles}]. \quad (32)$$

Examples

I. Because of rules (1) and (2) above Eq. (31), only two X diagrams contribute to $\langle 12 | W_2(\beta) | 1'2' \rangle$. These are shown in Fig. 2(e), and the corresponding expression for $\langle 12 | W_2(\beta) | 1'2' \rangle$ is

$$\langle 12 | \equiv_2(\beta) | 1'2' \rangle = \delta_{1,1'}\delta_{2,2'} + \int_0^\beta dt_1 \, {}^{\beta}\binom{1\,2}{1'2'}_{t_1}. \quad (33)$$

Now, according to the second of the Ursell equations (11), the operator $U_2(\beta,\beta')$ is given by

$$U_2(\beta,\beta') = W_2(\beta,\beta') - 1. \quad (34)$$

Upon comparing these last two equations, we see that the function $\langle 12 | U_2 | 1'2' \rangle$ of Eq. (16) is simply

$$U\binom{1\,2}{1'2'} = \int_0^\beta dt_1 \, {}^{\beta}\binom{1\,2}{1'2'}_{t_1} = \text{second symbol of Fig. 2(e)}, \quad (35a)$$

or

$$U_2(\beta) = \int_0^\beta dt_1 \, R(\beta,t_1). \quad (35b)$$

II. We next introduce the concept of a *connected X diagram*. A Qth-order connected X diagram for N particles is one in which all N vertical lines remain interconnected when the $(Q+1)$ horizontal lines are removed. Thus, the X diagram of Fig. 2(c) is connected. Now, if Eq. (35b) is substituted into Eqs. (29) for $N=3$, then one can verify with the aid of the third of the Ursell equations (11) (when written for Boltzmann statistics) that

$$U_3(\beta) = \sum_\mu \sum_{\nu \neq \mu} \int_0^\beta dt_2 \int_0^{t_2} dt_1 R_\mu(\beta,t_2) \times R_\nu(t_2,t_1) M_\nu^{(3)}(t_1). \quad (36a)$$

Upon taking matrix elements of Eq. (36a) one then verifies the following expression for $\langle 123 | U_3 | 1'2'3' \rangle$:

$$U\binom{1\,2\,3}{1'2'3'} = \sum_{Q=2}^{\infty} [\text{all different } Q\text{th-order, connected } X \text{ diagrams for 3 particles}]. \quad (36b)$$

III. The generalization of Eq. (36b) is that U_N is given by the sum over all connected, N-particle X diagrams. The ease with which we proved this result for $N=3$ was due to the fact that there were only a few unconnected X diagrams. However, in the case of $N=4$,

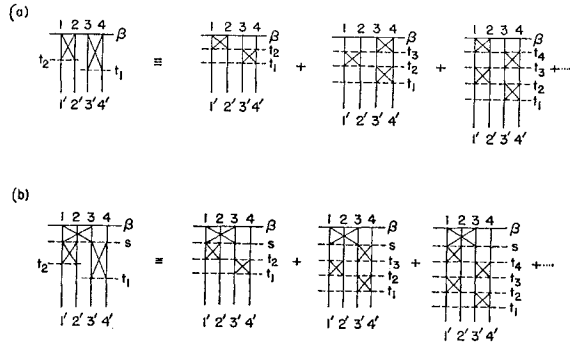

FIG. 3. (a) The diagrammatic representation of Eq. (39); (b) the diagrammatic representation of Eq. (39) with the replacement $\beta \to s$. In this case the leading factor $\int_0^\beta ds \, R_{13}(\beta,s)$ is missing from each of the terms of Eq. (39).

and for all higher values of N, there are an *infinite number* of unconnected X diagrams in

$$\langle 12\cdots N|W_N(\beta)|1'2'\cdots N'\rangle.$$

For example, all unconnected X diagrams of the type shown in Fig. 3(a) occur in $\langle 1234|W_4(\beta)|1'2'3'4'\rangle$.

We shall now show that the sum over all "unconnected products" in W_4 may be identified with the products U_2U_2 in the fourth of the Ursell equations (11). For this purpose we first write the operator product $(U_2)_\mu(U_2)_\nu$ for two *disjoint* pairs μ and ν as follows:

$$\begin{aligned}(U_2)_\mu(U_2)_\nu &= \int_0^\beta dt_2 dt_1 R_\mu(\beta,t_2)R_\nu(\beta,t_1) \\ &= \int_0^\beta dt_2\int_0^{t_2} dt_1[R_\mu(\beta,t_2)R_\nu(\beta,t_1)+R_\nu(\beta,t_2)R_\mu(\beta,t_1)].\end{aligned} \tag{37}$$

The operators R_μ and R_ν commute only when they are associated with disjoint pairs, i.e., when they are associated with four different sets of coordinates [they do not commute when $\mu=(1,2)$ and $\nu=(1,3)$].

Now, from Eqs. (28), (24), (34), and (35b), it follows that

$$R(t_3,t_1)=\left[1+\int_{t_2}^{t_3} ds\, R(t_3,s)\right]R(t_2,t_1) \tag{38}$$

for any value t_2. With the aid of this identity one may verify the following expansion for the first term in the second line of Eq. (37).

$$\begin{aligned}&\int_0^\beta dt_2\int_0^{t_2} dt_1\, R_\mu(\beta,t_2)R_\nu(\beta,t_1) \\ &= \int_0^\beta dt_2\int_0^{t_2} dt_1\, R_\mu(\beta,t_2)R_\nu(t_2,t_1) \\ &\quad+\int_0^\beta dt_3\int_0^{t_3} dt_2\int_0^{t_2} dt_1\, R_\nu(\beta,t_3)R_\mu(t_3,t_2)R_\nu(t_2,t_1) \\ &\quad+\int_0^\beta dt_4\int_0^{t_4} dt_3\int_0^{t_3} dt_2\int_0^{t_2} dt_1 \\ &\qquad\times R_\mu(\beta,t_4)R_\nu(t_4,t_3)R_\mu(t_3,t_2)R_\nu(t_2,t_1)+\cdots.\end{aligned} \tag{39}$$

Equation (39) is shown schematically in Fig. 3(a). If this equation is now substituted into Eq. (37), then one obtains

$$(U_2)_\mu(U_2)_\nu=\sum[\text{sum over all terms in the iteration of Eqs. (29) which depend only on the disjoint pairs } \mu \text{ and } \nu]. \tag{40}$$

By using Eqs. (35a), (36b), and (40) one may readily verify that the generalization of Eq. (36b) to the case $N=4$ is valid, through the isomorphism of terms in Eq. (32) for $N=4$ with the fourth of the Ursell equations (11).

IV. A *double-bond* in X diagrams is defined to be a structure in which two crosses are connected by the same two vertical lines, as shown in Fig. 2(d). There are no double bonds in Fig. 2(c). Now, the sum of Eq. (40) is a sum over a certain class of unconnected diagrams with double bonds [see Fig. 3(a)]. However, there is no reason why these diagrams must be unconnected, and in the next section we will also perform such sums over connected diagrams with double bonds. For example, by simply making the replacement $\beta\longrightarrow s$ in Eq. (39) one can obtain the sum whose matrix elements are shown in Fig. 3(b).

By an extension of the method used in example III, one can identify all of the unconnected X diagrams in Eqs. (32) for $N>4$ with corresponding product terms in the Nth of the Ursell equations (11). After making a series of induction proofs,[4] one finally obtains for the unsymmetrized cluster function U_N

$$U\begin{pmatrix}1\,2\cdots N\\ 1'2'\cdots N'\end{pmatrix} = \sum_{Q=N-1}^{\infty}[\text{all different } Q\text{th-order connected } X \text{ diagrams for } N \text{ particles}]. \tag{41}$$

Equation (41) is the generalization of Eq. (36b), and it is essentially equivalent to the result obtained by Lee and Yang.[10] In principle it permits one to calculate the T_N of Eq. (17), which are in turn necessary for an evaluation of $f^{(s)}$ via Eq. (21). However, the prescription of Eqs. (21) and (41) is unnecessarily complicated, as we shall now show by developing the linked-pair expansion of $f^{(s)}$.

As a preliminary to our further manipulations we make the observation that whenever a connected N-particle X diagram is written explicitly in terms of the two-particle symbols ${}^{t_2}(\ )_{t_1}$, cf. Eq. (31), that

$$\epsilon^{P_B}=\epsilon^N, \text{ for connected } N\text{-particle } X \text{ diagrams.} \tag{42}$$

The sign of the permutation of the bottom-row coordinates with respect to the top-row coordinates is equal to ϵ^N for a connected N-particle X diagram. Of course, if one uses only the notation of X diagrams in calculations, then this observation is unnecessary, since the definition (30) allows no ambiguity in the arrangement of bottom row coordinates with respect to top row coordinates: The sign in Eq. (31) is $+1$. We shall now adopt a different notation, however, in which Eq. (42) will be a quite useful relation. Equation (42) is

[10] The two-body operator $R(\beta,\beta')$ is not the same as the binary kernel $B(\beta-\beta')$ used by Lee and Yang. In terms of our notation, $B(\beta-\beta')=\exp(-\beta H_0^{(2)})[(\partial/\partial\beta)U_2(\beta,\beta')]\exp(\beta' H_0^{(2)})$. It is a simple matter to verify that when written in terms of $B(\beta-\beta')$, our Eq. (41) is equivalent to the general prescription of (LY I).[2]

verified by examining some simple X diagrams, and then generalizing to arbitrary X diagrams by making induction proofs.

Dashed-Line Cluster Graphs

Let Π be a permutation which simultaneously permutes the same sets of top and bottom row indices of a function, e.g.

$$\Pi_{12}\binom{1\,2}{1'2'}=\binom{2\,1}{2'1'}.$$

One may then verify from their definitions that since the N-particle Hamiltonian is symmetric in its N variables that all of the U_N and W_N functions of Sec. I are invariant under any permutation of the type Π. In particular:

$$\Pi U\binom{1\,2\cdots N}{1'2'\cdots N'}=U\binom{1\,2\cdots N}{1'2'\cdots N'}. \tag{43}$$

If this result is used in Eq. (17), then one may obtain an alternate form for T_N.

$$T\binom{1\,2\cdots N}{1'2'\cdots N'} =\epsilon^N(N!)^{-1}\sum_{P,P'}\epsilon^{P+P'}PP'U\binom{1\,2\cdots N}{1'2'\cdots N'}. \tag{44}$$

Thus, the $T_N\neq U_N{}^{(s)}$ are symmetrized matrix elements of the operators $U_N(\beta)$.

From Eqs. (44) and (41), we conclude that we may directly determine the T_N by taking symmetrized matrix elements of Eqs. (29) and then subtracting all unconnected U products. To represent the terms which occur in T_N, we shall introduce the notation of cluster graphs, which are essentially symmetrized combinations of X diagrams. Moreover, it is immediately clear that only symbols for the symmetrized matrix elements of the operator $R(t_2,t_1)$ will be necessary in these graphs. We shall call such matrix elements pair functions.

$$\left[\begin{matrix}1\,2\\1'2'\end{matrix}\right]_{t_1}^{t_2}\equiv\binom{1\,2}{1'2'}_{t_1}^{t_2}+\epsilon\binom{1\,2}{2'1'}_{t_1}^{t_2}\equiv\text{a pair function} =\langle 12|R(t_2,t_1)|1'2'\rangle+\epsilon\langle 12|R(t_2,t_1)|2'1'\rangle. \tag{45}$$

The basic unit of a cluster graph is a symbol for the pair function of Eq. (45) in the momentum representation (which representation we shall henceforth use) and we shall call such a symbol a *cluster vertex*. At any cluster vertex there must be two incoming and two outgoing lines, equipped with arrows, which correspond to the four momenta of the pair function. In these symbols we distinguish between *internal* (**l**) and *external* (**k**) momenta by drawing the internal momentum lines as dashed lines and the external momentum lines as solid lines. Only the lower temperature label t_i is attached to a cluster vertex, since the upper temperature label of the corresponding pair function is always t_{i+1} (or β). Two examples of cluster vertices are shown in Figs. 4(a) and 4(b).

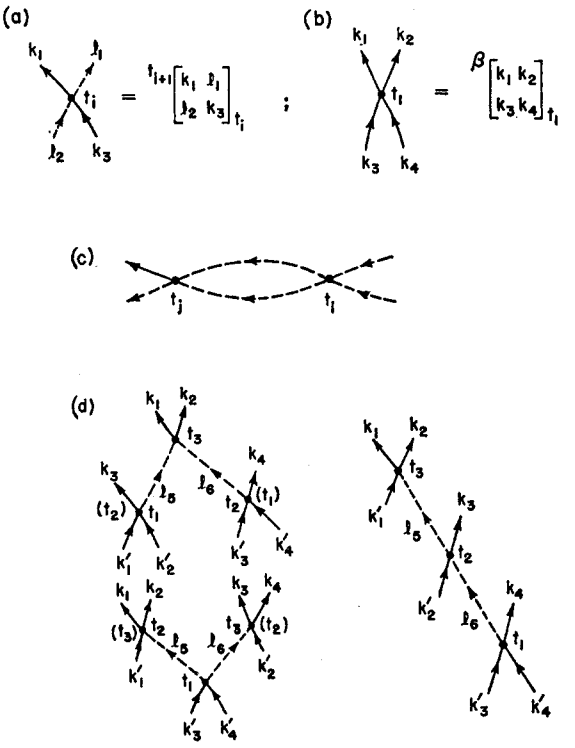

FIG. 4. (a) An example of a cluster vertex in the dashed-line formulation of cluster graphs; (b) a cluster vertex with no internal momentum lines; (c) a double bond in cluster graphs; (d) the five different, third order 4-particle dashed-line cluster graphs [see expressions (46)] for fixed assignments of the external **k** momenta.

A Qth-order, N-particle, *dashed-line cluster graph* is defined to be a set of Q cluster vertices which are entirely interconnected by $(2Q-N)$ dashed lines. The rules for connecting the Q cluster vertices of a dashed-line cluster graph, together with the prescriptions for writing down the corresponding expression are as follows:

1. It must not be possible to complete a loop in a cluster graph by following the arrows on dashed lines. Cluster graphs therefore always have a braided structure as shown in Fig. 5.

2. Every dashed line is attached to a cluster vertex at each end, so that the temperature variable t_i at the tail end is less than the temperature variable t_j at the head end. Moreover the Q temperature variables are labelled so that

$$0<t_1<t_2<\cdots<t_Q<t_{Q+1}\equiv\beta.$$

3. A *double bond* in a cluster graph is defined to be a structure in which two dashed lines connect the same two vertices [of Fig. 4(c)]. In this case the temperature variables t_i and t_j must be attached so that $t_{i+1}<t_j$.

4. Associate with each of the $(2Q-N)$ internal lines and the $2N$ external lines an integer $i(i=1, 2, \cdots, 2Q+N)$ and a corresponding momentum $\mathbf{l}_i$, $\mathbf{k}_i$ or $\mathbf{k}_i'$ according to whether the line is internal, outgoing external, or incoming external.

5. Two dashed-line cluster graphs are different if they cannot be topologically (including the relative positions of the *external momentum* and the *temperature* labels) deformed into each other.

6. For any given assignment of the temperature labels, the temperature integrations $\int_0^\beta dt_Q \int_0^{t_Q} dt_{Q-1} \cdots \int_0^{t_2} dt_1$ must be performed over the corresponding pair functions.

7. When the cluster graph is written in terms of the associated pair functions, (a) a factor of ϵ^{P_B} is included, where P_B is the total permutation of the bottom-row momenta (both external and internal) with respect to the top-row momenta; (b) a factor of $\frac{1}{2}$ is included for each double bond; (c) the sum over the $(2Q-N)$ internal momentum (and spin) coordinates is performed.

In Fig. 4(d) we exhibit the five possible third-order 4-particle cluster graphs for fixed assignments of the external $\mathbf{k}$ momenta. Their explicit expressions are as follows:

$$\sum_{\mathbf{l}_5\mathbf{l}_6} \int_0^\beta dt_3 \int_0^{t_3} dt_2 \int_0^{t_2} dt_1 \begin{bmatrix} \mathbf{k}_1 \mathbf{k}_2 \\ \mathbf{l}_5 \ \mathbf{l}_6 \end{bmatrix}_{t_3}^{\beta} \begin{bmatrix} \mathbf{l}_6 \ \mathbf{k}_4 \\ \mathbf{k}_3' \mathbf{k}_4' \end{bmatrix}_{t_2}^{t_3} \begin{bmatrix} \mathbf{k}_3 \ \mathbf{l}_5 \\ \mathbf{k}_1' \mathbf{k}_2' \end{bmatrix}_{t_1}^{t_2},$$

$$\sum_{\mathbf{l}_5\mathbf{l}_6} \int_0^\beta dt_3 \int_0^{t_3} dt_2 \int_0^{t_2} dt_1 \begin{bmatrix} \mathbf{k}_1 \mathbf{k}_2 \\ \mathbf{l}_5 \ \mathbf{l}_6 \end{bmatrix}_{t_3}^{\beta} \begin{bmatrix} \mathbf{k}_3 \ \mathbf{l}_5 \\ \mathbf{k}_1' \mathbf{k}_2' \end{bmatrix}_{t_2}^{t_3} \begin{bmatrix} \mathbf{l}_6 \ \mathbf{k}_4 \\ \mathbf{k}_3' \mathbf{k}_4' \end{bmatrix}_{t_1}^{t_2},$$

$$\sum_{\mathbf{l}_5\mathbf{l}_6} \int_0^\beta dt_3 \int_0^{t_3} dt_2 \int_0^{t_2} dt_1 \begin{bmatrix} \mathbf{k}_1 \ \mathbf{k}_2 \\ \mathbf{k}_1' \ \mathbf{l}_5 \end{bmatrix}_{t_3}^{\beta} \begin{bmatrix} \mathbf{k}_3 \mathbf{k}_4 \\ \mathbf{l}_6 \mathbf{k}_2' \end{bmatrix}_{t_2}^{t_3} \begin{bmatrix} \mathbf{l}_5 \ \mathbf{l}_6 \\ \mathbf{k}_3' \mathbf{k}_4' \end{bmatrix}_{t_1}^{t_2},$$

$$\sum_{\mathbf{l}_5\mathbf{l}_6} \int_0^\beta dt_3 \int_0^{t_3} dt_2 \int_0^{t_2} dt_1 \begin{bmatrix} \mathbf{k}_3 \mathbf{k}_4 \\ \mathbf{l}_6 \mathbf{k}_2' \end{bmatrix}_{t_3}^{\beta} \begin{bmatrix} \mathbf{k}_1 \ \mathbf{k}_2 \\ \mathbf{k}_1' \ \mathbf{l}_5 \end{bmatrix}_{t_2}^{t_3} \begin{bmatrix} \mathbf{l}_5 \ \mathbf{l}_6 \\ \mathbf{k}_3' \mathbf{k}_4' \end{bmatrix}_{t_1}^{t_2},$$

$$\sum_{\mathbf{l}_5\mathbf{l}_6} \int_0^\beta dt_3 \int_0^{t_3} dt_2 \int_0^{t_2} dt_1 \begin{bmatrix} \mathbf{k}_1 \ \mathbf{k}_2 \\ \mathbf{k}_1' \ \mathbf{l}_5 \end{bmatrix}_{t_3}^{\beta} \begin{bmatrix} \mathbf{l}_5 \ \mathbf{k}_3 \\ \mathbf{k}_2' \ \mathbf{l}_6 \end{bmatrix}_{t_2}^{t_3} \begin{bmatrix} \mathbf{l}_6 \ \mathbf{k}_4 \\ \mathbf{k}_3' \mathbf{k}_4' \end{bmatrix}_{t_1}^{t_2}. \tag{46}$$

The right-hand side of Eq. (44) for T_N may now be rewritten as a sum over all different cluster graphs:

$$T\begin{pmatrix} 1\,2\cdots N \\ 1'2'\cdots N' \end{pmatrix} = \sum_{Q=N-1}^{\infty} [\text{all different } Q\text{th-order } N\text{-particle dashed-line cluster graphs}]. \tag{47}$$

Equation (47) can be verified by referring to the remarks below Eq. (44), and by using Eqs. (44), (41), and (42). Alternatively, by using Eq. (45) for each pair function, Eq. (47) can be expanded to give $[\sum_{P'}(\epsilon^{N+P'})P']$ times Eq. (41).

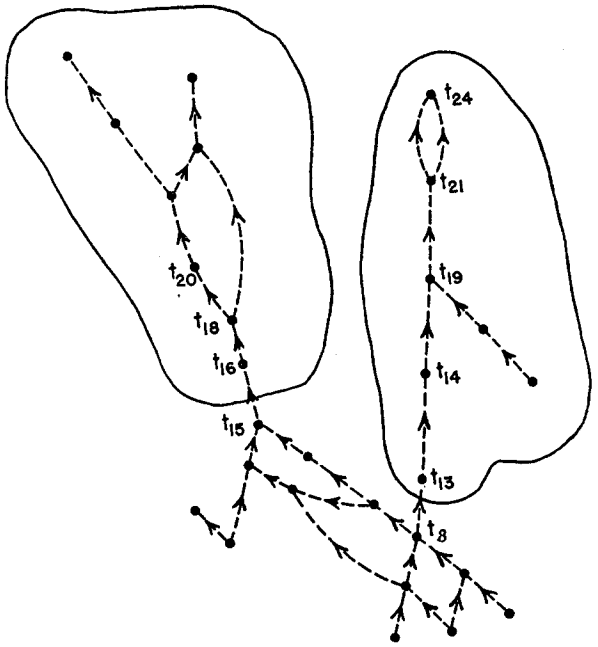

FIG. 5. A cluster graph with 28 vertices in the dashed-line formulation. For convenience the external lines and some of the temperature labels have been omitted. The encircled regions are proper cluster parts.

III. WIGGLY-LINE CLUSTER GRAPHS

The calculation of T_N in terms of dashed-line cluster graphs, Eq. (47), is already a great simplification over the method of calculation with X diagrams, Eqs. (17) and (41). In this section, we shall show that further simplification is possible by performing the sums over all double-bonds in dashed-line cluster graphs. When this is done, we will find that the prescription for the resulting "wiggly-line cluster graphs" will be a simple geometrical one. More important, however, the sums over double-bonds are a necessary, preliminary step to the work described in the following paper.

For reasons of simplicitly, we shall write down only operator expressions for cluster-graphs in the first part of this section, and we shall indicate this fact by the symbol $\approx$ in equations. We shall begin our considerations by writing down operator expressions for the first set of cluster graphs of Fig. 4(d), which we have redrawn in Figs. 6(a) and 6(b).

[Cluster graph of Fig. 6(a)]

$$\approx \int_0^\beta dt_3 \int_0^{t_3} dt_2 \int_0^{t_2} dt_1 \, R_A(\beta,t_3) R_B(t_3,t_2) R_C(t_2,t_1), \tag{48}$$

[Cluster graph of Fig. 6(b)]

$$\approx \int_0^\beta dt_3 \int_0^{t_3} dt_2 \int^{t_2} dt_1 \, R_A(\beta,t_3) R_C(t_3,t_2) R_B(t_2,t_1).$$

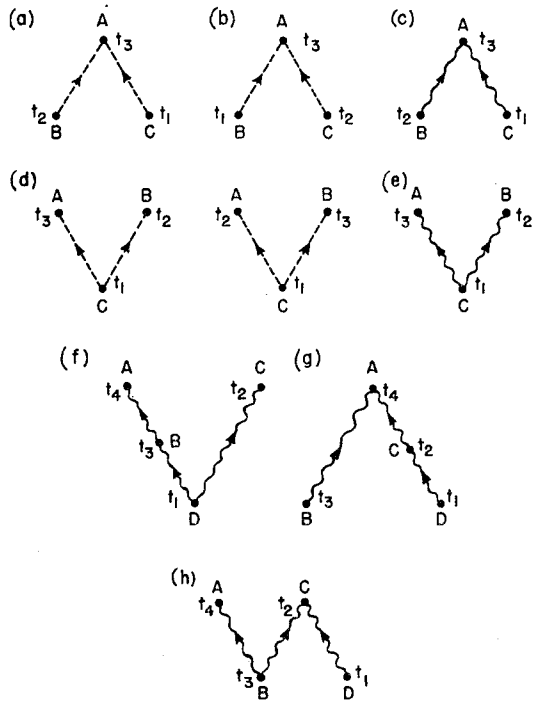

FIG. 6. (a) A third order, 4-particle cluster graph with dashed lines, [see Eq. (48)]. (b) The other possible temperature labelling of the cluster graph of Fig. (a) [see Eq. (48)]. (c) The cluster graph of Figs. (a) or (b) with the dashed lines replaced by wiggly lines [see Eq. (50)]. (d) The second set of third order, 4-particle cluster graphs with dashed lines. (e) The wiggly-line cluster graph, see Eq. (51), which corresponds to the dashed-line cluster graphs of Fig. (d). (f) A fourth order, 5-particle cluster graph with wiggly lines [see Eq. (52)]. (g) Another fourth order, 5-particle cluster graph with wiggly lines. (h) The fourth order, 5-particle cluster graph with wiggly lines of Eq. (53). For convenience, the external lines have been omitted from each of these cluster graphs.

We next consider the sum of dashed-line cluster graphs indicated in Fig. 7, which is analogous to the X-diagram sum of Fig. 3(b).

$$\int_0^\beta dt_3 \int_0^{t_3} dt_2 \int_0^{t_2} dt_1\, R_A(\beta,t_3)R_B(t_3,t_2)R_C(t_3,t_1)$$

$$\approx [\text{sum of cluster-graphs of Fig. 7}]. \quad (49)$$

We see that Fig. 6(a) is merely the first term of the series that consists of all possible dashed-line cluster graphs which differ only in the number of double-bonds along the two branches $(A-B)$ and $(A-C)$, and in which the temperature variable t_1 is associated with the lowest C vertex. We note that because of the rules for including double bonds in dashed-line cluster graphs, the number of double bonds along the branch $(A-C)$ minus the number of double bonds along the branch $(A-B)$ can only be zero or one.

We now define the wiggly-line cluster graph of Fig. (6c) to be the sum of Eq. (49) plus the corresponding

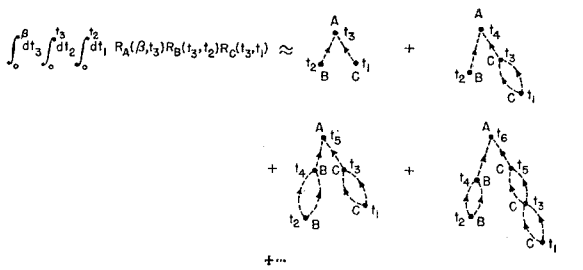

FIG. 7. The sum over dashed-line cluster graphs of the type in Fig. 6(a), which differ only in the number of double-bonds along the branches $(A-B)$ and $(A-C)$. In each of these cluster graphs the temperature variable t_1 is associated with the lowest (C) vertex. For convenience, the external lines have been omitted from each cluster graph.

equation which has Fig. 6(b) as its leading term.

[Cluster graph of Fig. 6(c)]

$$\approx \int_0^\beta dt_3\, R_A(\beta,t_3) \int_0^{t_3} dt_2 dt_1\, R_B(t_3,t_2)R_C(t_3,t_1)$$

$$= \int_0^\beta dt_3 \int_0^{t_3} dt_2 \int_0^{t_2} dt_1\, R_A(\beta,t_3)[R_B(t_3,t_2)R_C(t_3,t_1) + R_C(t_3,t_2)R_B(t_3,t_1)]. \quad (50)$$

When all possible ways of including double bonds in a cluster graph have been summed and all possible ways of ordering the temperature labels have been included, we shall draw a cluster graph for the resulting expression with wiggly lines instead of dashed lines, as with Eq. (50).

Proper Cluster Parts

The motivation for performing the sums of Eqs. (49) and (50) to obtain wiggly-line cluster graphs can be understood by examining Fig. 5. Consider, for example, the cluster vertices labelled (18), (19), and (20). According to the rules for writing down dashed-line cluster graphs, the corresponding temperature variables are associated with the integrations $\cdots \int_0^{t_{21}} dt_{20} \int_0^{t_{20}} dt_{19} \int_0^{t_{19}} dt_{18} \cdots$. Therefore, the two regions enclosed by the wiggly lines in Fig. 5 have a complicated interdependence of their temperature variables.

We define a *proper cluster part* as a part of a cluster graph which is connected to the rest of the cluster graph by only one incoming and/or one outgoing dashed line. (There may be any number of solid line connections.) The encircled regions in Fig. 5 are therefore proper cluster parts. We shall show that after the sum over all possible ways of including double bonds and over all orderings of the temperature variables has been made for a given dashed-line cluster graph, that the only temperature variables which proper cluster parts then have in common with the rest of their cluster graphs are those at the connecting vertices. Thus, the temperature variables which the encircled

proper cluster parts of Fig. 5 will have in common with the rest of the (wiggly-line) cluster graphs will be only t_{13} and t_{16}. In the following paper we shall need to know the temperature dependence of a proper cluster part independently of the rest of its cluster graph, and it is mainly for this reason that we are here performing the sums over double bonds. The fact that the resulting prescription for writing down wiggly-line cluster graphs will be simpler than the prescription for dashed-line cluster graphs is merely an added bonus.

The "disentangling" of the temperature dependences of proper cluster parts is very much related to the identification of product terms of the Ursell equations (11) for Boltzmann statistics, as they are contained in Eqs. (29) or (32). Thus, Eqs. (49) and (39), or Figs 7. and 3, are quite similar. Moreover, we see from Eqs. (49) and (50) that after summing over all possible ways of including double bonds and over both ways of ordering the temperature variables t_1 and t_2, the "upper" temperature labels for *both* the vertices B and C become t_3. The temperature dependences of the "proper cluster parts" B and C are no longer interrelated except through the variable t_3 of the vertex A where they are attached.

We next consider the dashed-line cluster graphs of Fig. 6(d). In this case, it is important to note that Eq. (39) remains valid even when the same arbitrary function of t_1 is included in the integrand of every term. Because of this fact, one can readily show that the sum over all possible ways of including double bonds along the branches $(A-C)$ and $(B-C)$ of the cluster graphs of Fig. 6(d) leads to the result:

[Cluster graph of Fig. 6(e)]

$$\approx\int_0^\beta dt_3\int_0^{t_3} dt_2\int_0^{t_2} dt_1[R_A(\beta,t_3)R_B(\beta,t_2)R_C(t_2,t_1)+R_B(\beta,t_3)R_A(\beta,t_2)R_C(t_2,t_1)]$$

$$=\int_0^\beta dt_3 R_A(\beta,t_3)\left[\int_0^{t_3} dt_2\int_0^{t_2} dt_1 R_B(\beta,t_2)R_C(t_2,t_1)+\int_{t_3}^\beta dt_2\int_0^{t_3} dt_1 R_B(\beta,t_2)R_C(t_3,t_1)\right]$$

$$=\int_0^\beta dt_3 R_A(\beta,t_3)\int_0^{t_3} dt_1\left[\int_{t_1}^{t_3} dt_2 R_B(\beta,t_2)R_C(t_2,t_1)+\int_{t_3}^\beta dt_2 R_B(\beta,t_2)R_C(t_3,t_1)\right]. \quad (51)$$

We see that when two proper cluster parts with *incoming* dashed lines (the vertices A and B) attach at a common vertex C, that they do not "attach independently" as we might have expected. There is an ordering preserved, even after the sum over all ways of including double bonds has been performed, which is that the upper temperature label at the vertex C is always the lesser of the set $\{t_2,t_3\}$.

We next determine what changes occur in Eqs. (50) and (51) when a fourth vertex is included, i.e., when the cluster graphs become 5-particle graphs instead of 4-particle ones. One finds the following results:

$$[\text{Cluster graph of Fig. 6(f)}]\approx\int_0^\beta dt_4\int_0^{t_4} dt_3 R_A(\beta,t_4)R_B(t_4,t_3)\int_0^{t_3} dt_1$$

$$\times\left[\int_{t_1}^{t_3} dt_2 R_C(\beta,t_2)R_D(t_2,t_1)+\int_{t_3}^\beta dt_2 R_C(\beta,t_2)R_D(t_3,t_1)\right]. \quad (52)$$

In this case the quantity

$$R_{AB}(\beta,t_3)\equiv\int_{t_3}^\beta dt_4 R_A(\beta,t_4)R_B(t_4,t_3)$$

can effectively be considered to be a single vertex, in which case Eq. (52) reduces to Eq. (51). A similar result is found for the wiggly-line cluster graph of Fig. 6(g). An important fourth order, five-particle cluster graph to investigate is the remaining simple case which we shall treat, namely:

$$[\text{Cluster graph of Fig. 6(h)}]\approx\int_0^\beta dt_4 R_A(\beta,t_4)\int_0^{t_4} dt_3$$

$$\times\left\{\int_{t_3}^{t_4} dt_2 R_C(\beta,t_2)R_B(t_2,t_3)\int_0^{t_2} dt_1 R_D(t_2,t_1)+\int_{t_4}^\beta dt_2 R_C(\beta,t_2)R_B(t_4,t_3)\int_0^{t_2} dt_1 R_D(t_2,t_1)\right\}. \quad (53)$$

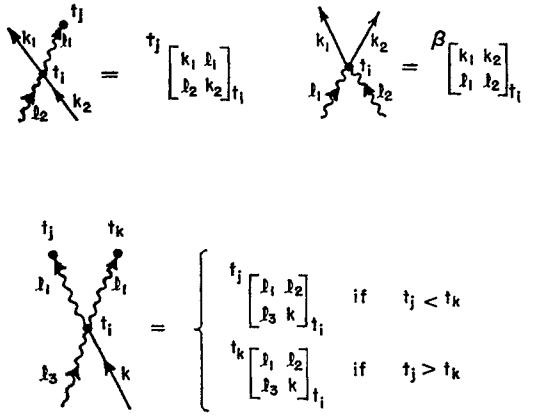

FIG. 8. Three examples of cluster vertices in the wiggly-line formulation of cluster graphs. The upper temperature labels of the corresponding pair functions are determined by the nature of the outgoing lines and the labels of the other vertices where the wiggly lines (if any) attach.

If the vertex D is removed, then Eq. (53) reduces to Eq. (51). When the vertex D is included, it "hangs freely" from the vertex C.

Equation (53) can be described in words. Start with the vertex A and write down its pair function $R_A(\beta,t_4)$ (or ${}^{\beta}[A]_{t_4}$). The final integration to be performed will be $\int_0^{\beta}dt_4$. Consider next the vertex B. Its pair function is $R_B(s,t_3)$, where we cannot yet specify the temperature label s, since two wiggly lines *leave* the vertex B. However, the t_3 integration, to be performed next to last, is $\int_0^{t_4}dt_3$. Consider next the vertex C, whose pair function is $R_C(\beta,t_2)$. The t_2-integration region must be broken into two parts $\int_{t_3}^{t_4}dt_2$ and $\int_{t_4}^{\beta}dt_2$, where t_4 is the temperature label at the vertex A. For the first part, the temperature label $s=t_2$, and for the second part $s=t_4$. Finally, consider the vertex D. Its pair function is $R_D(t_2,t_1)$ and its integration region is $\int_0^{t_2}dt_1$.

It is important to note that the description of the last paragraph also follows from Eqs. (50) and (51). It is a geometrical prescription for the expression on the right-hand side of Eq. (53), since it can be written down by only looking at the corresponding cluster graph of Fig. 6(h). Finally, we note that it was not essential, but merely convenient, to begin with the vertex A. We can apply Eqs. (50) and (51) to the determination of the expression (53) no matter what order we choose to do the four temperature integrations.

Equations (50), (51), (52), and (53) comprise all of the cases which need to be studied in order to understand the wiggly-line formulation of cluster graphs. We shall present this formulation, which is nothing more than a generalization of the above description of Eq. (53), before discussing the validity of using wiggly-line cluster graphs in Eq. (47) to calculate T_N.

Wiggly-Line Cluster Graphs

The basic unit of a wiggly-line cluster graph is again a symbol for the pair function of Eq. (45), and we shall again call this symbol a *cluster vertex*. In this case, the lower temperature label t_i of the pair function is again attached to the cluster vertex, but now, unlike the case of dashed-line cluster vertices, the upper temperature label is determined by the nature of the outgoing lines and the labels at the other vertices where the wiggly lines (if any) attach, as shown in Fig. 8. For example, if both outgoing lines are solid (external) lines, then the upper temperature label is β. The wiggly lines represent internal $\mathbf{l}$ momenta.

A Qth-order, N-particle, *wiggly-line cluster graph* is defined to be a set of Q cluster vertices which are entirely interconnected by $(2Q-N)$ wiggly lines. The rules for connecting the Q cluster vertices of a wiggly-line cluster graph together with the prescriptions for writing down the corresponding expression are as follows:

1. It must not be possible to complete a loop in a cluster graph by following the arrows on wiggly lines.

2. Double-bonds in wiggly-line cluster graphs, i.e., structures of the type shown in Fig. 4(c), are not allowed.

3. Every wiggly line is attached to a cluster vertex at each end, so that the temperature variable t_i at the tail end is less than the temperature variable t_j at the head end.

4. Associate with each of the $(2Q-N)$ internal lines and the $2N$ external lines an integer $i(i=1, 2, \cdots, 2Q-N)$ and a corresponding momentum $\mathbf{l}_i$, $\mathbf{k}_i$, or $\mathbf{k}_i'$ according to whether the line is internal, outgoing external, or incoming external.

5. Two wiggly-line cluster graphs are different if they cannot be topologically (including the relative positions of the *external momentum* labels) deformed into each other.

The next two rules determine the integration regions for the Q temperature variables of a Qth-order wiggly-line cluster graph.

6. Superimpose a grid of vertical lines on the cluster graph so that one and only one of its vertices falls between any two of the vertical lines. The cluster graph must also be drawn so that the vertex at the tail end of every wiggly line is lower than the vertex at the head end. The cluster graph of Fig. 5 has been redrawn in Fig. 9 according to these requirements, and we note that its vertices are now ordered (arbitrarily of course) from right to left. The Q vertices are to be labelled from right to left starting with t_1 and ending with t_Q. The labels can, however, be placed along the bottom of the grid of vertical lines to avoid cluttering the complicated parts of the cluster graph.

7. The determination of the integration limits of the Q temperature variables is now very simple. Two horizontal lines are drawn above and below the cluster graph and labelled by β and 0. The integration region for each variable t_i is then that part of the region $0<t_i<\beta$ which is consistent with rule 3 above. For

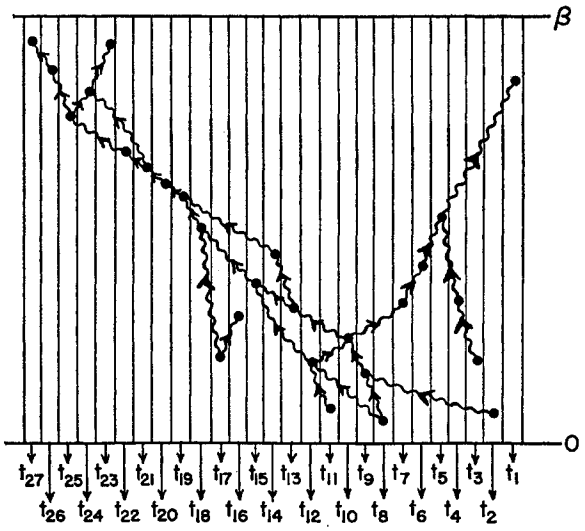

FIG. 9. The cluster graph of Fig. 5 redrawn in the wiggly-line formulation. For convenience, the external lines have been omitted. Note that either the vertex (21) or the vertex (24) of Fig. 5 cannot occur here, because there are no double bonds in wiggly-line cluster graphs.

example, in Fig. 9 we can start at the left end of the cluster graph and obtain for the integration limits of each variable the result:

$$\int_0^\beta dt_{27}\int_0^{t_{27}} dt_{26}\int_0^{t_{26}} dt_{25}\int_{t_{25}}^\beta dt_{24}\int_{t_{24}}^\beta dt_{23}\int_0^{t_{25}} dt_{22}\int_0^{t_{22}} dt_{21}\cdots \int_{t_{12}}^{t_{13}} dt_{10}\cdots\int_0^{t_9} dt_2\int_{t_5}^\beta dt_1.$$

These integration regions must sometimes be subdivided, however, for reasons which are typified by the example of Fig. 9.

(a) The integration region t_{14} in Fig. 9 must be subdivided according to whether $t_{14}>t_{15}$ or $t_{14}<t_{15}$. The t_{13}-integration region is then

$$\int_0^{t_{15}} dt_{13}\cdots {}^{t_{15}}\Big[\ \Big]_{t_{13}}\cdots \quad \text{when} \quad t_{15}<t_{14},$$

and

$$\int_0^{t_{14}} dt_{13}\cdots {}^{t_{14}}\Big[\ \Big]_{t_{13}}\cdots \quad \text{when} \quad t_{15}>t_{14}.$$

We have explicitly included the pair function corresponding to the t_{13} cluster vertex here, because its upper temperature label also varies according to whether $t_{14}>t_{15}$ or $t_{14}<t_{15}$. The dots represent the rest of the expression for the cluster graph.

(b) The t_{16}-integration region in Fig. 9 must be subdivided as follows:

$$\int_{t_{17}}^{t_{18}} dt_{16}\cdots {}^{\beta}\Big[\ \Big]_{t_{16}}\,{}^{t_{16}}\Big[\ \Big]_{t_{17}}\cdots$$

and

$$\int_{t_{18}}^{\beta} dt_{16}\cdots {}^{\beta}\Big[\ \Big]_{t_{16}}\,{}^{t_{18}}\Big[\ \Big]_{t_{17}}\cdots.$$

This situation is analogous to the t_2-integration regions of Eqs. (51), (52) and (53). The t_{22}-integration region in Fig. 9 does *not* have to be subdivided, however, because we always have $t_{22}<t_{24}$. Thus, the t_{21} integration is of the form:

$$\int_0^{t_{22}} dt_{21}\cdots {}^{t_{22}}\Big[\ \Big]_{t_{21}}\cdots.$$

The final two rules which we must give for wiggly-line cluster graphs are:

(8) When the cluster graph is written in terms of its associated pair functions, then (a) a factor of ϵ^{P_B} is included, where P_B is the total permutation of bottom-row momenta (both internal and external) with respect to top-row momenta; (b) the sum over the $(2Q-N)$ internal momentum (and spin) variables is performed.

The above rules completely specify the wiggly-line cluster graphs. From rules (6) and (7) it is evident that the temperature dependence of a proper cluster part is now indeed only related to the rest of its cluster graph by the temperature variable(s) at the connecting vertex (or vertices). From Fig. 9, for example, we can write the temperature dependence of the proper cluster part made up of the vertices (7), (6), (5), (4), (3), and (1) as follows:

$$f(t_7)=\int_{t_7}^\beta dt_6\int_{t_6}^\beta dt_5\int_0^{t_5} dt_4\int_0^{t_4} dt_3\int_{t_5}^\beta dt_1\ {}^{t_6}\Big[\ \Big]_{t_7}\,{}^{t_5}\Big[\ \Big]_{t_6}\,{}^{t_1}\Big[\ \Big]_{t_5}\,{}^{t_5}\Big[\ \Big]_{t_4}\,{}^{t_4}\Big[\ \Big]_{t_3}\,{}^{\beta}\Big[\ \Big]_{t_1}.$$

There is, of course, also a t_7 dependence contained in the rest of the cluster graph through the vertex (10).

Equation (47) for T_N will now be written in terms of wiggly-line cluster graphs

$$T\begin{pmatrix}1\,2\cdots N\\ 1'2'\cdots N'\end{pmatrix} = \sum_{Q=N-1}^{\infty}[\text{all different } Q\text{th-order } N\text{-particle wiggly-line cluster graphs}]. \quad (54)$$

The general verification of Eq. (54), i.e., that the sum over all dashed-line N-particle cluster graphs equals the sum over all wiggly-line N-particle cluster graphs, is rather complicated. It is made by generalizing the method outlined at the beginning of this section with a series of induction proofs. In particular, one can begin by generalizing Eq. (52) to the case of M vertices along the branch from A to D [see Fig. 6(f)]. When all possible ways of including double bonds between these vertices and between the vertices C and D, together with all possible ways of ordering the temperature

labels, have been summed, then one can show that the resulting expression has the same form as Eq. (52). The M vertices along the branch A to D can effectively be considered to be a single vertex. One can then proceed with an examination of even more general cases. We shall not give the general proof of Eq. (54), but rather shall content ourselves with its partial justification as presented at the beginning of this section. We note that the complete proof of Eq. (54) can be viewed as a generalization of the proof of Eq. (41) through the identification of unconnected U products in Eq. (32) [compare Figs. 3(a) and 3(b), for example].

IV. THE LINKED-PAIR EXPANSION OF $f^{(s)}$

The linked-pair expansion of the grand potential $f^{(s)}$ is derived by substituting Eq. (54) into Eq. (21). We first observe that for 2-particle cluster graphs Eq. (54) reduces to

$$T\begin{pmatrix}\mathbf{k}_1\,\mathbf{k}_2\\ \mathbf{k}_1'\mathbf{k}_2'\end{pmatrix}=\int_0^\beta dt\,\left[\begin{matrix}\mathbf{k}_1\,\mathbf{k}_2\\ \mathbf{k}_1'\mathbf{k}_2'\end{matrix}\right]_t, \tag{55}$$

which according to Eqs. (45) and (35a) is the same as Eq. (16). Therefore, the result of substituting Eq. (54) into Eq. (21) does not lead to any changes for the contracted 0-graphs which contain only 2-particle cluster graphs.

We next consider the result of substituting Eq. (54) for $N=3$ into the third contracted 0-graph of Fig. 1. In this case one obtains:

$$\begin{aligned}&[\text{Third contracted 0-graph of Fig. 1}]\\ &=\tfrac{1}{6}\sum_{\mathbf{k}_1\mathbf{k}_2\mathbf{k}_3}(\epsilon\nu_1)(\epsilon\nu_2)(\epsilon\nu_3)T\begin{pmatrix}\mathbf{k}_1\mathbf{k}_2\mathbf{k}_3\\ \mathbf{k}_1\mathbf{k}_2\mathbf{k}_3\end{pmatrix}\\ &=\sum_{\mathbf{k}_1\mathbf{k}_2\mathbf{k}_3 l}(\epsilon\nu_1)(\epsilon\nu_2)(\epsilon\nu_3)\Big\{\int_0^\beta dt_2\int_0^{t_2}dt_1\Big(\epsilon\left[\begin{matrix}\mathbf{k}_1\mathbf{k}_2\\ \mathbf{k}_1\,\mathbf{l}\end{matrix}\right]_{t_2}\left[\begin{matrix}\mathbf{l}\,\mathbf{k}_3\\ \mathbf{k}_2\mathbf{k}_3\end{matrix}\right]_{t_1}+\frac{1}{2}\left[\begin{matrix}\mathbf{k}_1\mathbf{k}_2\\ \mathbf{l}\,\mathbf{k}_3\end{matrix}\right]_{t_2}\left[\begin{matrix}\mathbf{l}\,\mathbf{k}_3\\ \mathbf{k}_1\mathbf{k}_2\end{matrix}\right]_{t_1}\Big)\\ &\qquad+\tfrac{1}{6}\sum_{Q=3}^{\infty}[\text{all different } Q\text{th-order, 3-particle, wiggly-line cluster graphs}]\Big\}.\end{aligned} \tag{56}$$

One sees that there are only two different second-order terms in Eq. (56), although one starts with nine terms in Eq. (54) (and with 36 terms in the X-diagram notation). The relabelling of $\mathbf{k}$ momenta in contracted 0-graphs leads to very large numbers of identical terms.

We now state the general result which one obtains when Eq. (54) is substituted into Eq. (21) and all terms are gathered together which become identical after relabelling of $\mathbf{k}$ momenta:

$$\begin{aligned}\Omega f^{(s)}(g,\Omega,\beta)=\Omega f_0^{(s)}(g,\Omega,\beta)\\ +\sum_{Q=1}^{\infty}[\text{all different } Q\text{th-order}\\ \text{linked-pair 0-graphs}].\end{aligned} \tag{57}$$

The proof of Eq. (57) will be given after we have defined Qth-order linked-pair 0-graphs.

For the purpose of studying the distribution functions of a system, such as the momentum distribution, it is necessary to define not only linked-pair 0-graphs, but also linked-pair ζ graphs for $\zeta>0$. We therefore define a *Qth-order, linked-pair ζ graph* ($\zeta=0,1,2\cdots$) to be a collection of Q cluster vertices [see Figs. 4(b) and 8], which are entirely interconnected by m solid lines and n wiggly lines, and which have ζ incoming external solid lines and ζ outgoing external solid lines, where $m+n+\zeta=2Q$. The rules for connecting the Q cluster vertices by the $(m+n)$ internal lines of a linked-pair ζ-graph, and the procedures for determining the corresponding expression are as follows:

(i) When connecting the $(m+n)$ internal lines to the Q vertices, the n wiggly lines must be connected to cluster vertices according to rules (1), (2), and (3) for wiggly-line cluster graphs (Sec. III).

(ii) Two linked-pair ζ graphs are different if their topological structures, including line types and directions, are different.

(iii) Associate with each internal line a different integer $i(i=1,2,\cdots,m+n)$ and a corresponding momentum $\mathbf{k}_i$ or $\mathbf{l}_i$ according to whether the line is solid or wiggly.

(iv) If $\zeta\neq 0$, then associate the external lines with certain pre-given momenta.

(v) According to rules (i)–(iv), every linked-pair ζ graph consists of connected wiggly-line cluster graphs. For each cluster graph, perform the integrations over the temperature variables of its cluster vertices according to rules (6) and (7) for wiggly-line cluster graphs (Sec. III).

(vi) Assign a factor $\epsilon\nu_k$, where ν_k is given by Eq. (20), to each *internal* solid line.

(vii) Assign a factor S^{-1} to the entire linked-pair graph, where

$$S=\text{symmetry number}. \tag{58}$$

The symmetry number S is defined to be the total number of permutations of the m integers associated

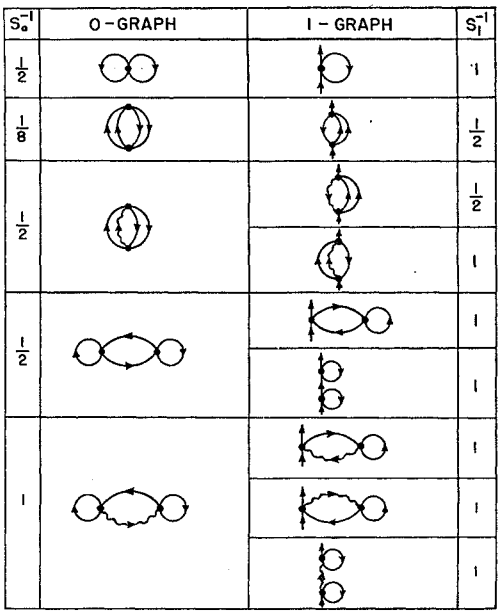

FIG. 10. In the second column are shown the one and two vertex linked-pair 0-graphs. By cutting lines in these graphs, one obtains the corresponding linked-pair 1 graphs shown in the third column. The inverse symmetry number has been included with each graph, but the temperature labels of the vertices have been omitted for convenience.

with the *solid* internal lines that leave the graph topologically (including the positions of these numbers relative to the m solid internal lines) unchanged.

(viii) Assign a factor ϵ^{P_B} to the graph, where P_B is the total permutation of the $2Q$ bottom-row momenta of the pair functions with respect to the $2Q$ top-row momenta.

(ix) Finally, sum over all $(m+n)$ internal momentum (and spin) coordinates.

According to the above definition, Qth-order linked-pair ζ graphs contain Q pair functions, Eq. (45). In Fig. 10, we have drawn all of the one- and two-vertex linked-pair ζ graphs for $\zeta=0$ and $\zeta=1$. With each graph we have included its associated symmetry number. Now, the only two-pair terms which occur in the grand potential, Eq. (21), are those given by Eq. (56), and the two contracted 0-graphs which are products of two T_2 functions. But these four terms can also be described by linked-pair 0-graphs, cf. Fig. 10. Therefore, both the $Q=1$ and $Q=2$ terms of Eq. (57) are correct. Moreover, a tedious examination of all the three-pair terms in the grand potential leads to the conclusion that the 29, $Q=3$ terms of Eq. (57) are also correct.

The general proof that Eq. (57) is correct proceeds in analogy with the proof in Appendix A of (LY IV).[3] Let us *assign* a different integer $i(i=1, 2\cdots m)$ to every solid internal line of a (contracted or linked-pair) ζ graph. The resulting graph is called a *numbered* ζ graph *generated* from the original ζ graph. Two numbered ζ graphs are different only if they have different topological structures, including the positions of the numbers relative to the solid lines.

Let D be the total number of different numbered ζ graphs which can be generated from the same ζ graph. From the definition of the symmetry number given below Eqs. (18) or (58), it is easy to see that

$$D=(m!)S^{-1}. \tag{59}$$

We may therefore deduce the following result:

$$\sum[\text{all different } \zeta \text{ graphs with } m \text{ solid internal lines}] = (m!)^{-1}\sum[\text{all different numbered } \zeta \text{ graphs with } m \text{ solid internal lines}], \tag{60}$$

since after appropriately relabelling the $\mathbf{k}$ momenta corresponding to the solid internal lines, the D different numbered ζ graphs of Eq. (59) have identical expressions. Equation (60) is true for both contracted ζ graphs and linked-pair ζ graphs. We next substitute Eq. (54) for each of the vertex factors in a contracted ζ graph to obtain

$$\sum[\text{all different contracted, numbered } \zeta \text{ graphs with } m \text{ solid internal lines}] = \sum[\text{all different linked-pair, numbered } \zeta \text{ graphs with } m \text{ solid internal lines}]. \tag{61}$$

Equation (61) follows from rule (5) in the definition of wiggly-line cluster graphs (Sec. III). We finally combine Eqs. (60) and (61) to arrive at

$$\sum[\text{all different contracted } \zeta \text{ graphs with } m \text{ solid internal lines}] = \sum[\text{all different linked-pair } \zeta \text{ graphs with } m \text{ solid internal lines}]. \tag{62}$$

Equation (57) is now obtained by substituting Eq. (62) into Eq. (21), as was to be proved.

Examples

We give below a few examples of the expressions for linked-pair 0-graphs.

1. A linked-pair 0-graph which includes the cluster of Fig. 6(e), see Eq. (51), is shown in Fig. 11(a). The corresponding expression is:

$$[\text{Linked-pair 0-graph of Fig. 11(a)}] = \tfrac{1}{2}\sum_{\mathbf{k}_1\mathbf{k}_2\mathbf{k}_3\mathbf{k}_4}\sum_{\mathbf{l}_5\mathbf{l}_6}\nu_1\nu_2\nu_3\nu_4\int_0^\beta dt_3\int_0^{t_3}dt_2\Big\{\int_{t_2}^{t_3}dt_1\begin{bmatrix}\beta\\ \mathbf{k}_1\mathbf{k}_2\\ \mathbf{k}_1\mathbf{l}_5\end{bmatrix}_{t_3}\begin{bmatrix}t_1\\ \mathbf{l}_5\mathbf{l}_6\\ \mathbf{k}_2\mathbf{k}_3\end{bmatrix}_{t_2}\begin{bmatrix}\beta\\ \mathbf{k}_3\mathbf{k}_4\\ \mathbf{l}_6\mathbf{k}_4\end{bmatrix}_{t_1} + \int_{t_3}^{\beta}dt_1\begin{bmatrix}\beta\\ \mathbf{k}_1\mathbf{k}_2\\ \mathbf{k}_1\mathbf{l}_5\end{bmatrix}_{t_3}\begin{bmatrix}t_3\\ \mathbf{l}_5\mathbf{l}_6\\ \mathbf{k}_2\mathbf{k}_3\end{bmatrix}_{t_2}\begin{bmatrix}\beta\\ \mathbf{k}_3\mathbf{k}_4\\ \mathbf{l}_6\mathbf{k}_4\end{bmatrix}_{t_1}\Big\}. \tag{63}$$

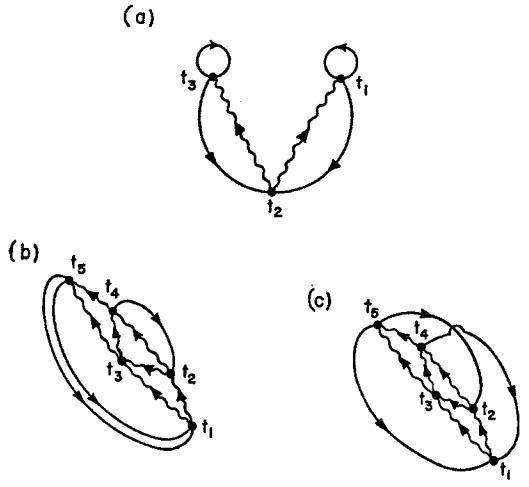

FIG. 11. (a) The third order 4-particle linked-pair 0-graph of Eq. (63); (b) a fifth order 3-particle linked-pair 0-graph, see Eq. (65a); (c) the other fifth order 3-particle linked-pair 0-graph, see Eq. (65b).

After relabelling variables, the second line of this expression is found to be equal to the first line, but it does not seem to be of value to exploit this symmetry by introducing further rules for our graphs. If the sums over double bonds had not been performed, then in the corresponding dashed-line expression, the last pair function in the first line of Eq. (63) would have been

$$^{t_3}\begin{bmatrix}\mathbf{k}_3\mathbf{k}_4\\ \mathbf{l}_6\mathbf{k}_4\end{bmatrix}_{t_1},$$

whereas the first pair function of the second line would have been

$$^{t_1}\begin{bmatrix}\mathbf{k}_1\mathbf{k}_2\\ \mathbf{k}_1\ \mathbf{l}_5\end{bmatrix}_{t_3};$$

see third and fourth lines of (46).

We shall show in the next section that for a short-range force in the scattering length ($=a_s$) approximation,

$$^{t_2}\begin{bmatrix}\mathbf{k}_1\ \mathbf{k}_2\\ \mathbf{k}_1'\mathbf{k}_2'\end{bmatrix}_{t_1}=\delta^{(3)}(\mathbf{k}_1+\mathbf{k}_2-\mathbf{k}_1'-\mathbf{k}_2')(\text{constants})\times a_s[1+O(k_{12}\times\text{range})^2]. \quad (64)$$

This means that the pair function is independent of temperature to first approximation. Therefore, in the calculation of physical quantities which depend on only one, two, and three pair terms, the dashed-line cluster graphs lead to the same expressions as the wiggly-line cluster graphs, because the derivation of Eq. (62) did not depend on the difference between these two kinds of cluster graphs. For example, the calculation of the energy of a Fermi gas to third order in the parameter (k_Fa_s), where k_F is the Fermi momentum, is equally well calculated with either wiggly-line or dashed-line linked-pair 0-graphs. On the other hand, it is essential to use the wiggly-line linked-pair 1 graphs in the calculation of the momentum distribution of a Fermi gas, as we shall show in the following paper.

2. In Eq. (56) we saw that there were only two different second order, 3-particle linked-pair 0-graphs. One can show, more generally, that there are only two different Qth-order, 3-particle linked-pair 0-graphs. This is a special feature of the three-body problem. For example, the two fifth order 3-particle linked-pair 0-graphs are shown in Figs. 11(b) and 11(c). Their explicit expressions are:

[Linked-pair 0-graph of Fig. 11(b)]

$$=\tfrac{1}{2}\sum_{\mathbf{k}_1\mathbf{k}_2\mathbf{k}_3}\sum_{\mathbf{l}_4\mathbf{l}_5\cdots\mathbf{l}_{10}}\nu_1\nu_2\nu_3\int_0^\beta dt_5\int_0^{t_5}dt_4\int_0^{t_4}dt_3\int_0^{t_3}dt_2\int_0^{t_2}dt_1\ ^{\beta}\begin{bmatrix}\mathbf{k}_1\mathbf{k}_2\\ \mathbf{l}_4\ \mathbf{l}_5\end{bmatrix}_{t_5}\times\ ^{t_5}\begin{bmatrix}\mathbf{k}_3\mathbf{l}_4\\ \mathbf{l}_6\mathbf{l}_7\end{bmatrix}_{t_4}\ ^{t_4}\begin{bmatrix}\mathbf{l}_5\mathbf{l}_6\\ \mathbf{l}_8\mathbf{l}_9\end{bmatrix}_{t_3}\ ^{t_3}\begin{bmatrix}\mathbf{l}_7\ \mathbf{l}_8\\ \mathbf{l}_{10}\mathbf{k}_3\end{bmatrix}_{t_2}\ ^{t_2}\begin{bmatrix}\mathbf{l}_9\mathbf{l}_{10}\\ \mathbf{k}_1\mathbf{k}_2\end{bmatrix}_{t_1}, \quad (65a)$$

[Linked-pair 0-graph of Fig. 11(c)]

$$=\sum_{\mathbf{k}_1\mathbf{k}_2\mathbf{k}_3}\sum_{\mathbf{l}_4\mathbf{l}_5\cdots\mathbf{l}_{10}}\nu_1\nu_2\nu_3\int_0^\beta dt_5\int_0^{t_5}dt_4\int_0^{t_4}dt_3\int_0^{t_3}dt_2\int_0^{t_2}dt_1\ ^{\beta}\begin{bmatrix}\mathbf{k}_1\mathbf{k}_2\\ \mathbf{l}_4\ \mathbf{l}_5\end{bmatrix}_{t_5}\times\ ^{t_5}\begin{bmatrix}\mathbf{k}_3\mathbf{l}_4\\ \mathbf{l}_6\mathbf{l}_7\end{bmatrix}_{t_4}\ ^{t_4}\begin{bmatrix}\mathbf{l}_5\mathbf{l}_6\\ \mathbf{l}_8\mathbf{l}_9\end{bmatrix}_{t_3}\ ^{t_3}\begin{bmatrix}\mathbf{l}_7\ \mathbf{l}_8\\ \mathbf{l}_{10}\mathbf{k}_1\end{bmatrix}_{t_2}\ ^{t_2}\begin{bmatrix}\mathbf{l}_9\mathbf{l}_{10}\\ \mathbf{k}_2\mathbf{k}_3\end{bmatrix}_{t_1}. \quad (65b)$$

In this case, the expressions for the wiggly-line and dashed-line linked-pair 0-graphs are the same, because there are no ways of including double-bonds between the vertices of the corresponding dashed-line cluster graphs.

There is a close connection between Eq. (57) for the grand potential and the corresponding expression derived by Bloch and DeDominicis.[5] In order to demonstrate this connection, it is necessary to replace our expansion in terms of the pair-function (45) by a development in terms of the potential $\mathbf{V}_2(t)$ of Eq. (26), since the results of Bloch and DeDominicis are expressed in terms of the latter quantities. According to Eqs. (28) and (25), the operator $R(t_2,t_1)$ can be expanded

in terms of the two-body potential by iterating an equation for $W_2(t_2,t_1)$:

$$R(t_2,t_1)=-W_2(t_2,t_1)\mathbf{V}(t_1)$$
$$W_2(t_2,t_1)=1-\int_{t_1}^{t_2} ds\, W_2(t_2,s)\mathbf{V}(s). \tag{66}$$

With the aid of Eqs. (66) it is possible to determine the precise correspondence between our Eq. (57) and the results obtained by Bloch and DeDominicis. For example, one first notes that in the latter work, factors of $\epsilon\nu_k$ and $(1+\epsilon\nu_k)$ are assigned to lines according to the temperature integration limits, whereas we have introduced two kinds of lines and then assigned factors of $\epsilon\nu_k$ only to the solid lines. One may, however, rewrite our rules for linked-pair 0-graphs so as to explicitly exhibit the line factors of Bloch and DeDominicis. If this is done, then one finds that there is still a difference between the two theories, because we have no graphs with "wiggly-line double bonds," whereas the prescription of Bloch and DeDominicis includes such graphs. Iteration of Eqs. (66) at every vertex finally achieves the exact correspondence, by introducing into our theory all of the missing graphs.

V. THE TWO-BODY PROBLEM

In the previous sections we have shown that the grand potential of quantum statistics can be expressed entirely in terms of the matrix elements of the two-body operator $R(t_2,t_1)$, where according to Eqs. (28), (34), and (23),

$$R(t_2,t_1)=-\frac{\partial}{\partial t_1}U_2(t_2,t_1),$$
$$U_2(t_2,t_1)=\exp(t_2H_0^{(2)})\exp[-(t_2-t_1)H^{(2)}]\times\exp(-t_1H_0^{(2)})-1. \tag{67}$$

We shall first determine the matrix elements of $U_2(t_2,t_1)$ in the momentum representation for $\Omega\to\infty$ and for a general, spin-independent, central interaction. Our procedure will be to make a partial-wave decomposition of the plane wave matrix elements $\langle\mathbf{k}_1\mathbf{k}_2|\,U_2(t_2,t_1)\,|\mathbf{l}_1\mathbf{l}_2\rangle$ and to express each partial wave in terms of the two-particle reaction matrix (the A matrix). Thus, one can show that

$$\langle\mathbf{k}_1m_1,\mathbf{k}_2m_2|\,U_2(t_2,t_1)\,|\mathbf{l}_1n_1,\mathbf{l}_2n_2\rangle$$
$$=\frac{(2\pi)^6}{\Omega^2}\delta^{(3)}(\mathbf{k}_1+\mathbf{k}_2-\mathbf{l}_1-\mathbf{l}_2)\delta_{m_1n_1}\delta_{m_2n_2}\frac{2}{(2\pi)^3}\sum_{L=0}^{\infty}(2L+1)P_L(\hat{n}_k\cdot\hat{n}_1)\langle k|\,U_L(t_2,t_1)\,|l\rangle, \tag{68}$$

where $\hat{n}_k$ is a unit vector in the direction $\mathbf{k}=\frac{1}{2}(\mathbf{k}_2-\mathbf{k}_1)$, $\hat{n}_1$ is a unit vector in the direction $\mathbf{l}=\frac{1}{2}(\mathbf{l}_2-\mathbf{l}_1)$, $P_L(\cos\theta)$ is a Legendre polynomial, $(2\pi)^6/\Omega^2$ is a factor needed to convert momentum state sums to integrals, m_1, m_2, n_1, and n_2 are spin-state magnetic quantum numbers, and $U_L(t_2,t_1)$ is the radial part of the two-body operator $U_2(t_2,t_1)$ for the Lth partial wave. The state vectors $|k\rangle$ and $|l\rangle$ are defined in the position representation by the expressions:

$$\langle k|r\rangle\equiv(2\pi)^{\frac{1}{2}}k^{-1}F_L(kr),$$
$$F_L(\rho)=\rho j_L(\rho)\underset{\rho\to\infty}{\longrightarrow}\sin(\rho-\tfrac{1}{2}L\pi), \tag{69}$$

where $j_L(\rho)$ is the spherical Bessel function.

The true radial state vector $\langle r|k_0L\rangle$, corresponding to the energy eigenvalue $\omega(k_0L)\equiv\hbar^2k_0^2/m$, obeys the radial wave equation

$$\left[\frac{d^2}{dr^2}+k_0^2-\frac{L(L+1)}{r^2}\right]\langle r|k_0L\rangle=U(r)\langle r|k_0L\rangle, \tag{70}$$

where $U(r)=(m/\hbar^2)V(r)$ is the two-body interaction. It is regular at the origin and has the asymptotic form

$$\langle r|k_0L\rangle\underset{r\to R}{\longrightarrow}(2/R)^{\frac{1}{2}}\sin[k_0R-\tfrac{1}{2}L\pi+\delta_L(k_0)]. \tag{71}$$

In Eq. (71), R is the radius of a large spherical box and $\delta_L(k_0)$ is the phase shift for the Lth partial wave. One cannot determine a general expression for the radial state vector, or even for the phase shifts. However, the radial state vector can be expressed in terms of the two-body reaction matrix or A matrix, which is then given for any particular interaction by a single integral. Thus, if one defines the A matrix in terms of the radial state vector by the equation

$$\langle r|k_0L\rangle=\left(\frac{2}{R}\right)^{\frac{1}{2}}\cos\delta_L(k_0)\left\{F_L(k_0r)+2\pi^{-1}P\int_0^\infty kdk\,F_L(kr)\left[\frac{\langle k|A^{(L)}|k_0\rangle}{k^2-k_0^2}\right]\right\}, \tag{72}$$

then one finds that the expression for the A matrix is simply

$$(2/R)^{\frac{1}{2}}\cos\delta_L(k_0)\langle k|A^{(L)}|k_0\rangle=-k^{-1}\int_0^\infty dr\,F_L(kr)U(r)\langle r|k_0L\rangle$$
$$=-(2\pi)^{-\frac{1}{2}}\int_0^\infty dr\langle k|r\rangle U(r)\langle r|k_0L\rangle, \tag{73}$$

$$\langle k|A^{(L)}|k\rangle=\tan\delta_L(k).$$

Essentially, the A matrix gives the correction to the free-particle state vector due to the interaction $U(r)$. In Eq. (72), P denotes the principle value of the integral. If bound states occur in the two-body problem, then we write the radial bound-state vectors as $\langle r|\gamma L\rangle$, and the corresponding energy eigenvalues as $\omega(\gamma L)=-\hbar^2\gamma^2/m$. In this case we define the Fourier transform of the states $\langle r|\gamma L\rangle$ by the equation

$$\langle r|\gamma L\rangle=\frac{2}{\pi}\int_0^\infty dk\,\phi_{\gamma L}(k)F_L(kr). \tag{74}$$

Using Eqs. (72) and (74), one can express the matrix elements $\langle k|U_L(t_2,t_1)|l\rangle$ in terms of the A matrix and any bound-state vectors as follows:

$$\langle k|U_L(t_2,t_1)|l\rangle=\left(\frac{2\pi}{k^2-l^2}\right)\{l^{-1}\langle k|A^{(L)}|l\rangle\cos^2\delta_L(l)e^{t_2(\omega_k-\omega_l)}-k^{-1}\langle l|A^{(L)}|k\rangle^*\cos^2\delta_L(k)e^{t_1(\omega_k-\omega_l)}\}$$
$$+\left(\frac{4}{k^2-l^2}\right)\int_0^\infty dq\,\cos^2\delta_L(q)e^{t_2(\omega_k-\omega_q)}e^{t_1(\omega_q-\omega_l)}\langle l|A^{(L)}|q\rangle^*\langle k|A^{(L)}|q\rangle\left[P\left(\frac{1}{l^2-q^2}\right)-P\left(\frac{1}{k^2-q^2}\right)\right]$$
$$+2\pi(kl)^{-1}\sum_\gamma\phi_{\gamma L}^*(l)e^{t_2(\omega_k-\omega_\gamma)}e^{t_1(\omega_\gamma-\omega_l)}\phi_{\gamma L}(k). \tag{75}$$

In order to derive Eq. (75), one must understand the principle value of the integral in Eq. (72) to mean the integral over the principle part of the integrand, where

$$P(1/x)=\mathrm{Re}\left(\frac{1}{x+i\epsilon}\right)=\frac{x}{x^2+\epsilon^2}. \tag{76}$$

Moreover, one can show that the following identity holds for the product of two principle parts

$$P(1/x)P(1/y)=(y-x)^{-1}[P(1/x)-P(1/y)]+\pi^2\delta(x)\delta(y), \tag{77}$$
$$\pi\delta(x)=\lim_{\epsilon\to0+}\left(\frac{\epsilon}{x^2+\epsilon^2}\right).$$

The derivation of Eq. (75) includes the use of this identity.

If the interaction $U(r)$ includes an infinite repulsive core, then, as Lee and Yang have shown, one must subtract from Eq. (75) a function which is proportional to $\phi(t_2-t_1)$, where $\phi(x)=0$ for $x>0$ is a step function. The reason is that according to Eq. (67) we must have $\langle\mathbf{k}_1\mathbf{k}_2|U_2(t_2,t_2)|\mathbf{k}_1\mathbf{k}_2\rangle\equiv0$. The step-function term can also be understood as a correction term arising because the hard core wave functions do not form a complete set of functions over all space. In the particular case of a pure repulsive core interaction, one can show that the S-wave part of Eqs. (68) and (75), corrected by the step-function term, reduces to the corresponding equation derived by Lee and Yang in reference 2.[11]

Equations (68) and (75), for the plane wave matrix elements of $U_2(t_2,t_1)$, give the T_2 function [see Eq. (55)] which results from a first temperature integration in the expression for a cluster graph, e.g., the t_2 integrations of Eq. (63) and the t_1 integrations of Eqs. (65). For all but one of the cluster vertices of a cluster graph, one needs, in addition, expressions for the plane wave matrix elements of $R(t_2,t_1)$. According to Eq. (67), these matrix elements can be obtained by simply differentiating the matrix elements of $U_2(t_2,t_1)$ with respect to t_1.

$$\langle\mathbf{k}_1m_1,\mathbf{k}_2m_2|R(t_2,t_1)|\mathbf{l}_1n_1,\mathbf{l}_2n_2\rangle$$
$$=\frac{(2\pi)^6}{\Omega^2}\delta^{(3)}(\mathbf{k}_1+\mathbf{k}_2-\mathbf{l}_1-\mathbf{l}_2)\delta_{m_1n_1}\delta_{m_2n_2}\frac{2}{(2\pi)^3}\sum_{L=0}^\infty(2L+1)P_L(\hat{n}_k\cdot\hat{n}_l)$$
$$\times[C_L(kl|t_2t_1)+B_L(kl|t_2t_1)+\delta(t_2-t_1)\langle k|U_L(t_2,t_2)|l\rangle], \tag{78}$$

where

$$C_L(kl|t_2t_1)=\left(\frac{2\pi\hbar^2}{m}\right)\frac{1}{k}\langle l|A^{(L)}|k\rangle\cos^2\delta_L(k)e^{t_1(\omega_k-\omega_l)}$$
$$+\left(\frac{2\pi\hbar^2}{m}\right)\left(\frac{2}{\pi}\right)\int_0^\infty dq\,\cos^2\delta_L(q)e^{t_2(\omega_k-\omega_q)}e^{t_1(\omega_q-\omega_l)}P\left(\frac{1}{k^2-q^2}\right)\langle l|A^{(L)}|q\rangle\langle k|A^{(L)}|q\rangle, \tag{79}$$

$$B_L(kl|t_2t_1)=\left(\frac{2\pi\hbar^2}{m}\right)\frac{1}{kl}\sum_\gamma\phi_{\gamma L}(l)(l^2+\gamma^2)e^{t_2(\omega_k-\omega_\gamma)}e^{t_1(\omega_\gamma-\omega_l)}\phi_{\gamma L}(k). \tag{80}$$

In these equations $\omega_k=\hbar^2k^2/m$ and $\omega_\gamma=-\hbar^2\gamma^2/m$. We have also assumed that the A matrix and any $\phi_{\gamma L}(k)$ are real functions, which is the case whenever the wave equation (70) is invariant under time-reversal. The $\delta(t_2-t_1)$ term is the derivative of the step-function term discussed above. It is zero for a finite repulsive core, but not for an infinite repulsive core. In either case, it is useful to include this term, for then substitution of

[11] Lee and Yang use the notation $U_2(t_2-t_1)=\exp[-(t_2-t_1)H^{(2)}]-\exp[-(t_2-t_1)H_0^{(2)}]$.

Eqs. (78)–(80) into Eq. (35a) yields the form of Eqs. (68) and (75) directly.

Although it is necessary to solve the two-body problem in order to completely determine the A matrix, there are physical systems such as dilute gases where a partial knowledge of the A-matrix suffices. For a gas of particles interacting with only short-range forces, it is sufficient to know only the scattering length and the effective range to first approximation. In this case the $L=0$ and $L=1$ A matrices can be expanded as follows:

$$q^{-1}\langle k|A^{(0)}|q\rangle=-[a_s+\tfrac{1}{2}(k^2+q^2)r_1{}^3+\tfrac{1}{2}(q^2-k^2)r_2{}^3+q^4O(\text{range})^5], \quad (81)$$
$$k^{-1}q^{-2}\langle k|A^{(1)}|q\rangle=-a_p{}^3[1+O(q\times\text{range})^2].$$

Since the A matrix is equal to the tangent of the phase shift on the energy shell, the lengths a_s, r_1, and a_p are scattering parameters defined as $a_s=S$-wave scattering length, $r_1{}^3=\frac{1}{2}a_s{}^2r_{\text{eff}}$, where $r_{\text{eff}}=$effective range, and $a_p=P$-wave scattering length, i.e.,

$$-a_p{}^3\equiv\lim_{k\to 0}k^{-3}\tan\delta_1(k). \quad (82)$$

The parameter r_2 is not a scattering parameter, but rather it depends upon the close-in behavior of the two-particle wave function. In absolute value, the order of magnitude of each of these four lengths is the interaction range.

The usefulness of expressing the matrix elements of $U_2(t_2,t_1)$ and $R(t_2,t_1)$ in terms of the A matrix is that for a dilute gas one can use Eqs. (81) for the leading terms in the expressions for the energy and other thermodynamic quantities. In the following paper, for example, we will show that in the calculation of the thermodynamic quantities of a Fermi gas, only the three scattering parameters a_s, r_1, and a_p enter to order $(k_F\times\text{range})^3$. This fact has also been successfully applied in the many-body pseudopotential method.[12]

It is possible to write down an explicit expression for the A matrix in the case of certain simple interactions. For example, the A matrix for a zero-range S-wave attraction outside of a repulsive core of diameter a is:

$$\langle k|A^{(0)}|q\rangle=-\frac{q}{k}\left[\frac{\sin ka+kb\cos ka}{\cos qa-qb\sin qa}\right][1+O(q^2/U_a)]$$
$$[\text{repulsive core}+\text{zero-range}\ (L=0)\ \text{attraction}], \quad (83)$$
$$\langle k|A^{(L)}|q\rangle=-\frac{qF_L(ka)}{kG_L(qa)}[1+O(q^2/U_a)]$$
$$[\text{pure repulsive core}],$$

where

$$G_L(\rho)=-\rho n_L(\rho)\underset{\rho\to\infty}{\longrightarrow}\cos(\rho-L\pi/2), \quad (84)$$

and the function $n_L(\rho)$ is the spherical Neumann function. The quantity $b<0$ is the scattering length due to the attraction alone, and U_a is the height of the repulsive core. In Table I we have tabulated the range parameters of Eqs. (81) for this interaction, as determined from Eqs. (83).

TABLE I. The low-energy expansion of the A matrix for a zero range S-wave attraction outside of a repulsive core.

$q^{-1}\langle k|A^{(0)}|q\rangle=-[a_s+\frac{1}{2}(k^2+q^2)r_1{}^3+\frac{1}{2}(q^2-k^2)r_2{}^3+q^4O(\text{range})^5]$.
$k^{-1}q^{-2}\langle k|A^{(1)}|q\rangle=-a_p{}^3[1+q^2O(\text{range})^2]$.

$a=$diameter of hard core; $b=$scattering length (<0) due to the attraction alone.

Parameter	Pure repulsive core	Repulsive core+zero-range attraction
a_s	a	$a+b$
$r_1{}^3=\frac{1}{2}a_s{}^2r_{\text{eff}}$	$\frac{1}{3}a^3$	$\frac{1}{3}[(a+b)^3-b^3]$
$r_2{}^3$	$\frac{2}{3}a^3$	$\frac{1}{3}[2(a+b)^3-b^2(a+b)+b^3]$
$a_p{}^3$	$\frac{1}{3}a^3$	$\frac{1}{3}a^3$

DISCUSSION

Recently, Kohn and Luttinger[13] have raised an important question concerning the role played by "anomalous," or improper graphs in the determination of the ground-state properties of a Fermi system. Improper graphs are Qth-order linked-pair graphs in which a group of $N<Q$ cluster vertices can be isolated so that there is only one incoming line and one outgoing line. Thus, in the Brueckner-Goldstone formalism[14] such graphs are excluded by assuming that their effect on the calculation of ground-state properties is only to give a modified energy-momentum relation for the fermions while still retaining the free-particle momentum distribution. In the present context, one can readily see that an examination of the question raised by Kohn and Luttinger is much more feasible once the sums of Sec. III over all cluster graphs with double bonds have been performed. The reason is that the "proper parts" of improper graphs will often be proper cluster parts, and in the wiggly-line cluster graphs the temperature dependence of proper cluster parts is only upon the one or two temperature variables at the connecting vertices. This feature greatly simplifies the further investigation of improper graphs, because a proper part can itself then be examined independently of the rest of its improper linked-pair graph.

The following paper consists of a detailed study of the way in which improper graphs contribute in the calculation of the low-temperature properties of a Fermi gas.

ACKNOWLEDGMENTS

The author is indebted to Professor B. A. Jacobsohn for his initial stimulation and ideas in this work, and to Professor T. D. Lee and Dr. F. J. Ernst for helpful criticism and suggestions.

[12] K. Huang and C. N. Yang, Phys. Rev. **105**, 767 (1957).

[13] W. Kohn and J. M. Luttinger, Phys. Rev. **118**, 41 (1960).

[14] J. Goldstone, Proc. Roy. Soc. (London) **A239**, 267 (1957).